Clinical Quantification of Myocardial Blood Flow Using PET: Joint Position Paper of the SNMMI Cardiovascular Council and the ASNC

Writing Group:
Venkatesh L. Murthy (cochair)[1], Timothy M. Bateman[2], Rob S. Beanlands[3], Daniel S. Berman[4], Salvador Borges-Neto[5], Panithaya Chareonthaitawee[6], Manuel D. Cerqueira[7], Robert A. deKemp[3], E. Gordon DePuey[8], Vasken Dilsizian[9], Sharmila Dorbala[10], Edward P. Ficaro[11], Ernest V. Garcia[12], Henry Gewirtz[13], Gary V. Heller[14], Howard C. Lewin[15], Saurabh Malhotra[16], April Mann[17], Terrence D. Ruddy[3], Thomas H. Schindler[18], Ronald G. Schwartz[19], Piotr J. Slomka[4], Prem Soman[20], and Marcelo F. Di Carli (cochair)[10]

[1]Frankel Cardiovascular Center, Division of Cardiovascular Medicine, Department of Internal Medicine, University of Michigan, Ann Arbor, Michigan; [2]Mid America Heart Institute, Kansas City, Missouri; [3]National Cardiac PET Centre, Division of Cardiology, University of Ottawa Heart Institute, Ottawa, Ontario, Canada; [4]Departments of Imaging and Medicine, Cedars-Sinai Medical Center, Los Angeles, California; [5]Division of Nuclear Medicine, Department of Radiology, and Division of Cardiology, Department of Medicine, Duke University School of Medicine, Duke University Health System, Durham, North Carolina; [6]Department of Cardiovascular Medicine, Mayo Clinic, Rochester, Minnesota; [7]Department of Nuclear Medicine, Cleveland Clinic, Cleveland, Ohio; [8]Division of Nuclear Medicine, Department of Radiology, Mt. Sinai St. Luke's and Mt. Sinai West Hospitals, Icahn School of Medicine at Mt. Sinai, New York, New York; [9]Department of Diagnostic Radiology and Nuclear Medicine, University of Maryland School of Medicine, Baltimore, Maryland; [10]Cardiovascular Imaging Program, Brigham and Women's Hospital, Boston, Massachusetts; [11]Division of Nuclear Medicine, University of Michigan, Ann Arbor, Michigan; [12]Department of Radiology and Imaging Sciences, Emory University, Atlanta, Georgia; [13]Massachusetts General Hospital and Harvard Medical School, Boston, Massachusetts; [14]Gagnon Cardiovascular Institute, Morristown Medical Center, Morristown, NJ, USA; [15]Cardiac Imaging Associates, Los Angeles, California; [16]Division of Cardiovascular Medicine, Jacobs School of Medicine and Biomedical Sciences, University at Buffalo, Buffalo, New York; [17]Hartford Hospital, Hartford, Connecticut; [18]Division of Nuclear Medicine, Department of Radiology, Johns Hopkins School of Medicine, Baltimore, Maryland; [19]Cardiology Division, Department of Medicine, and Nuclear Medicine Division, Department of Imaging Sciences, University of Rochester Medical Center, Rochester, New York; and [20]Division of Cardiology, Heart and Vascular Institute, University of Pittsburgh Medical Center, Pittsburgh, Pennsylvania

Expert Content Reviewers:
Andrew Einstein[1], Raymond Russell[2], James R. Corbett[3], SNMMI Cardiovascular Council Board of Directors, and ASNC Board of Directors

[1]Division of Cardiology, Department of Medicine, and Department of Radiology, Columbia University Medical Center and New York–Presbyterian Hospital, New York, New York; [2]Warren Alpert Medical School, Brown University, Providence, Rhode Island; and [3]Frankel Cardiovascular Center, Division of Cardiovascular Medicine, Department of Internal Medicine, and Division of Nuclear Medicine, Department of Radiology, University of Michigan, Ann Arbor, Michigan

PREAMBLE

Radionuclide myocardial perfusion imaging (MPI) is among the most commonly performed diagnostic tests in cardiology. Although the diagnostic and prognostic applications of radionuclide MPI are supported by a wealth of observational and clinical trial data, its performance is limited by two fundamental drawbacks. First, conventional MPI by SPECT and PET measures relative perfusion, that is, the assessment of regional myocardial perfusion relative to the region with the highest perfusion tracer uptake. This means that a global reduction in myocardial perfusion ("balanced" reduction of flow) may remain undetected and that, in general, the extent of coronary artery disease (CAD) is underestimated, as has been demonstrated with both ^{201}Tl- and ^{99m}Tc-labeled perfusion tracers (*1–3*). For example, Lima et al. found that in patients with severe 3-vessel CAD, ^{99m}Tc-sestamibi SPECT MPI showed perfusion defects in multivessel and typical 3-vessel-disease patterns in only 46% and 10% of patients, respectively (*2*). Similarly, it has been reported that only 56% of patients with left main CAD are identified as being at high risk by having more than 10% of the myocardium abnormal on stress SPECT MPI (*4*). Second, the ^{99m}Tc flow tracers available for SPECT MPI are inherently limited by a relatively low first-pass extraction fraction at high flow rates, thus limiting the precision and accuracy of these tracers for estimation of myocardial

Received Aug. 28, 2017; revision accepted Sep. 11, 2017.
For correspondence or reprints contact: Venkatesh L. Murthy, University of Michigan, 1338 Cardiovascular Center, SPC 5873, Ann Arbor, MI 48109.
E-mail: vlmurthy@med.umich.edu
Published online Dec. 14, 2017.
This article is being jointly published in the *Journal of Nuclear Cardiology* and *The Journal of Nuclear Medicine*.

DOI: 10.2967/jnumed.117.201368

blood flow (MBF) during stress (*5*). Clinical studies have shown that even small differences in extraction fraction can result in a clinical difference in the detection and quantification of myocardial ischemia by SPECT (*6,7*).

These drawbacks of SPECT are addressed by PET, with its ability to quantify global and regional MBF (in mL/min/g of tissue), assess regional perfusion abnormalities with relative MPI, and assess contractile function abnormalities and chamber dimensions with gated imaging. The purpose of this document is, first, to consolidate and update technical considerations for clinical quantification of MBF and myocardial flow reserve (MFR) from earlier documents (*8*) and, second, to summarize and update the scientific basis for their clinical application (*9,10*).

TECHNICAL CONSIDERATIONS

Perfusion Tracers

The available PET tracers for conventional MPI and quantitative MBF imaging are shown in Table 1. The most commonly used tracers are ^{82}Rb-chloride and ^{13}N-ammonia, with a small number of centers worldwide using ^{15}O-water. ^{18}F-flurpiridaz is currently under investigation, with one phase III trial completed and a second trial awaiting initiation. Because of their short half-lives, ^{13}N-ammonia and ^{15}O-water require an on-site cyclotron. In contrast, ^{18}F-flurpiridaz, because of its longer isotope half-life (~2 h), can be produced at regional cyclotron or radiopharmacy facilities and distributed as a unit dose. ^{82}Rb has a short half-life and is produced from an ^{82}Sr/^{82}Rb generator lasting 4–8 weeks (*11,12*), depending on initial activity and desired radiotracer activity. The short half-lives of ^{82}Rb and ^{15}O-water enable fast rest–stress imaging protocols (~20–30 min), but count statistics and standard MPI quality can be limited by the rapid isotope decay. ^{82}Rb also has a long positron range, but this does not limit the achievable spatial resolution in practice, because of image reconstruction postfiltering and cardiorespiratory motion. The radiation effective dose (mSv/GBq) is an order of magnitude lower for the short-lived isotopes than for ^{18}F-flurpiridaz; however, the dose absorbed by the patient can be lowered by reducing the total injected activity at the expense of longer imaging times for conventional MPI.

The physiologic properties of an ideal perfusion tracer for MBF quantification would include 100% extraction from blood to tissue, and 100% retention (no washout), resulting in a linear relationship between MBF and the measured tracer activity over a wide range. The currently available PET perfusion tracers, however, have limited (<100%) extraction and retention, resulting in a nonlinear (but still monotonic) relationship between MBF, tracer uptake, and retention rates as illustrated in Figure 1. ^{15}O-water and ^{13}N-ammonia have close to 100% initial (unidirectional) extraction over a wide range of MBF values, resulting in a tracer uptake rate (K_1) that is close to the true MBF (Fig. 1C). Rapid early washout reduces the tracer retention of ^{13}N-ammonia to approximately 50%–60% at peak stress MBF values. ^{15}O-water washes out so rapidly that there is effectively no tracer retention in cardiac tissue above the blood background level (Fig. 1D). ^{82}Rb has a substantially lower extraction fraction (~35% at peak stress) and tracer retention than does ^{13}N-ammonia. Although only limited data are available, ^{18}F-flurpiridaz appears to have extraction and retention values similar to or slightly higher than those of ^{13}N-ammonia (*13,14*). These physiologic properties of the particular perfusion tracer have a direct bearing on the optimal choice of kinetic model for image analysis and

TABLE 1
Properties of Radiotracers Used for PET MBF Quantification

Property	^{82}Rb-chloride	^{13}N-ammonia	^{15}O-water	^{18}F-flurpiridaz
Isotope production method	Generator	Cyclotron	Cyclotron	Cyclotron
Isotope half-life (min)	1.27	10	2.0	110
Positron range (mm) RMS	2.6	0.57	1.0	0.23
Image resolution (mm) FWHM	8	5	6	5
Effective dose (mSv/GBq)	1	2	1	20
Peak stress/rest* extraction (%)	35/70	95/100	100	95/100
Peak stress/rest* retention (%)	25/70	50/90	0	55/90
Spillover from adjacent organs	Stomach wall	Liver and lung	Liver	Early liver
Regulatory status	FDA-approved; 2 suppliers	FDA-approved; ANDA required for onsite production	Not FDA-approved	Phase 3 trials partially completed
Typical rest dose for 3D/2D (mCi†)	30/45	10/15	20/30	2/3
Typical stress dose for 3D/2D (mCi†)	30/45	10/15	20/30	6/7
Protocol features	Rapid protocol	Permits exercise‡; delay of 4–5 half-lives between rest and stress unless different doses used	Rapid protocol; no tracer retention for routine MPI	Permits exercise‡; different doses for rest and stress required

*Peak stress = 3–4 mL/min/g, rest = 0.75–1.0 mL/min/g.
†1 mCi = 37 MBq.
‡Exercise protocols do not allow quantification of MBF.
RMS = root mean square (standard) deviation; FWHM = full width at half maximum achievable using PET scanner with 5-mm spatial resolution; FDA = Food and Drug Administration; ANDA = abbreviated new drug application.

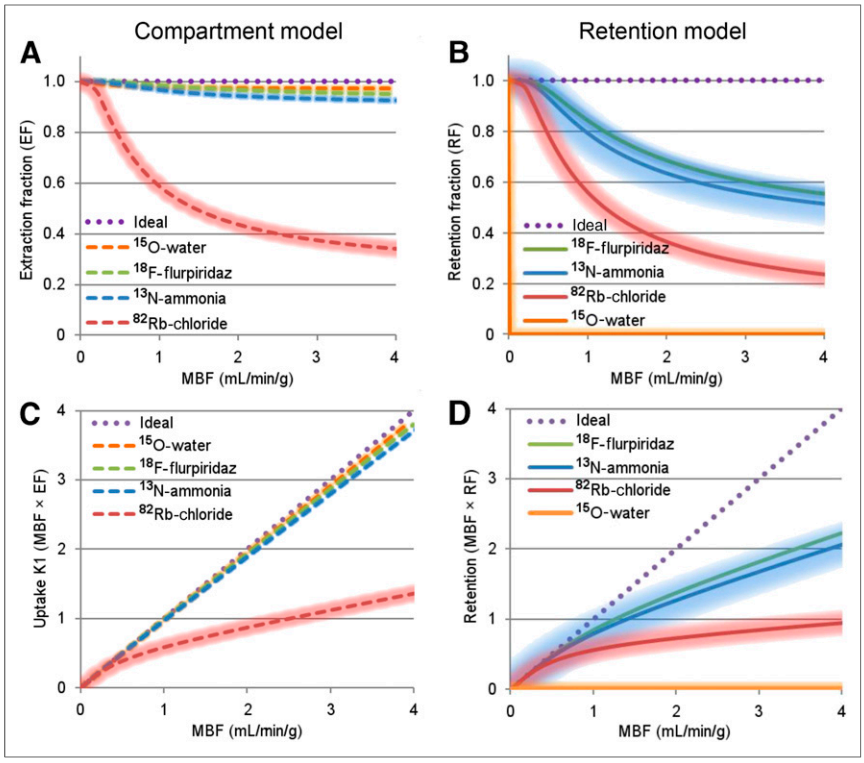

FIGURE 1. Radiotracer unidirectional extraction fractions (A) used with compartmental modeling of tracer uptake rates K_1 (C), and radiotracer retention fractions (B) used with simplified retention modeling of tracer net uptake (D). Underlying data were obtained from previous publications (*14,22,221,228,229*). Limited data suggest that properties of ^{18}F-flurpiridaz are similar to those of ^{13}N-ammonia. Shaded regions represent variability in reported values.

MBF quantification, as illustrated in Figure 2. Limited spatial resolution causes spillover or blurring of uptake signals from adjacent organs—an effect that varies somewhat between tracers and is a potential concern for accurate MBF quantification (Table 1).

Scanner Performance

Contemporary PET scanners operate in 3-dimensional (3D) acquisition mode, as opposed to the older 2-dimensional (2D) (or 2D/3D) systems that were constructed with interplane septa designed to reduce scatter. 3D systems generally require lower injected activity, with a concordant reduction in patient radiation effective dose. For the short-lived tracers ^{82}Rb and ^{15}O-water, injected activities of as high as 2,220–3,330 MBq (60–90 mCi) were commonly used with 2D PET systems. However, this amount of activity will cause detector saturation on 3D PET systems; therefore, the injected activity must be reduced to avoid these effects (*15*). Weight-based dosing may help to provide consistent image quality and accurate MBF quantification, but the maximum tolerated activity can vary greatly between 3D PET systems (*15*). Careful consideration should be given to optimizing injected doses to avoid detector saturation during the blood pool first-pass uptake phase while also preserving sufficient activity in the tracer retention (tissue) phase to allow high-quality images for MPI interpretation. The ultrashort half-life of ^{82}Rb is particularly challenging in this regard (Fig. 3). Importantly, detector saturation will generally result in falsely elevated MBF assessments due to underestimation of the blood input function. Newer solid-state detectors should further increase the dynamic range of 3D PET systems, reducing the need to trade off MPI quality for MBF accuracy.

Image Acquisition and Analysis

Quantification of MBF requires accurate measurement of the total tracer activity transported by the arterial blood and delivered to the myocardium over time. Measurements of arterial isotope activity versus time (time–activity curves) are typically acquired using image regions located in the arterial blood pool (e.g., left ventricle, atrium, or aorta). As only the tracer in plasma is available for exchange with the myocardial tissues, whole-blood–to–plasma corrections may be required to account for tracer binding to plasma proteins, red blood cell uptake, hematocrit, and appearance of labeled metabolites in the blood. For example, ^{13}N-labeled metabolites (urea, glutamine, glutamate) accumulate in the blood and account for 40%–80% of the total activity as early as 5 min after injection of ^{13}N-ammonia (*16*).

With older 2D PET systems, a single static scan may be adequate for accurate integration of the blood time–activity data (*17*), because dead-time losses and random rates are low and change relatively slowly over time. However, with current 3D PET systems, dead-time losses and random rates are much higher and more rapidly changing during the bolus first-pass transit; therefore, dynamic imaging with reconstruction of sequential short timeframes is typically required for accurate sampling and integration of the arterial blood activity. Some standardization of image acquisition and reconstruction protocols for accurate MBF quantification has occurred, but it is not universally applied. Dynamic frame-rates typically vary from 5 to 10 s during the first-pass transit through the heart and from 1 to 5 minutes during the later tissue phase. Minimal postreconstruction smoothing should be applied on the dynamic image series. Excess filtering increases adjacent organ spillover effects and can bias the MBF measurements.

In practice, list-mode acquisition is recommended because it allows flexibility in the timing and reconstruction of dynamic images for MBF, static images for MPI, electrocardiography-gated images for left ventricular ejection fraction, and respiration-gated images for quality assurance assessment of breathing artifacts. Further discussion can be found in the "Image Acquisition and Reconstruction Parameters" section. Scatter from intense or focal activity near the edge of the field of view can also bias the 3D scatter correction, leading to artifacts (*18*). Therefore, when using 3D PET, it is important to flush the tracer injection line with a volume of saline high enough to clear the tracer activity out of the cephalic, axillary, and subclavian veins.

To estimate MBF from dynamic PET images, time–activity curves are fit to a mathematic model describing the tracer kinetics over time (*19*). Various models have been proposed and evaluated, but the two most commonly used for ^{82}Rb and ^{13}N-ammonia are the 1-tissue-compartment model (*20*) and the simplified retention model (*17*). Both models have the same conceptual property of normalizing the late-phase myocardial activity to account for the total amount of tracer that was delivered by the arterial blood. An

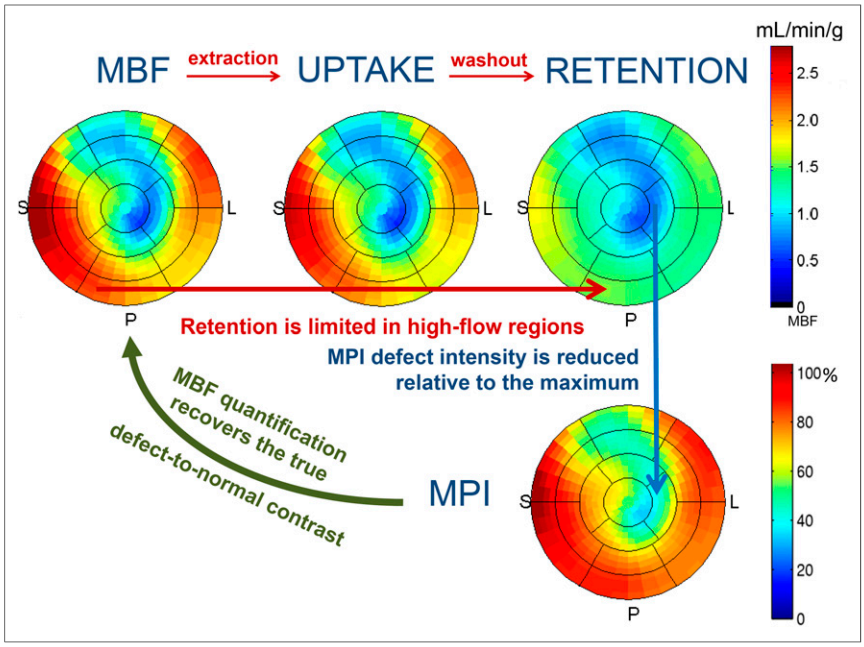

FIGURE 2. Polar maps demonstrating MBF, uptake, and retention along with their relationship to traditional relative MPI in example using ^{13}N-ammonia. Uptake of tracer is determined by local MBF. However, because most PET tracers have incomplete extraction at higher MBFs, tracer uptake in high-MBF regions may be reduced (note that intense red regions on MBF image are less intense on uptake image). Furthermore, tracer retention is usually limited in high-MBF regions. Consequently, contrast between high- and low-MBF regions is further reduced on retention images. Standard myocardial perfusion images are produced by normalizing retention images such that regions of greatest retention are scaled to 100%. This does not restore contrast between defect and normal regions. MBF quantification restores contrast and adds absolute scale (mL/min/g).

example analysis of a 1-tissue-compartment model is shown for a stress ^{13}N-ammonia PET scan in Figure 2. The MBF polar map is estimated using an assumed tracer-specific unidirectional extraction fraction dependent on MBF ($EF = 1 - e^{-PS/MBF}$, where PS is the permeability–surface area product) and the measured uptake rate constant (K_1/EF = MBF), as well as regional corrections for total blood volume (TBV) and partial-volume underestimation (1 – TBV) of the myocardial activity.

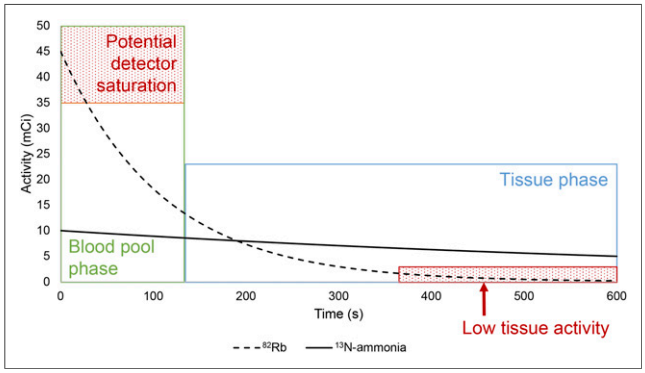

FIGURE 3. Decay of typical 370-MBq (10 mCi) dose of ^{13}N-ammonia (solid black line) and 1,665-MBq (45 mCi) dose of ^{82}Rb (dashed line). Because of the ultrashort half-life of ^{82}Rb, higher activities must be administered to ensure reasonable counting rates during delayed tissue-phase imaging (blue region) for generation of gated and static images for MPI interpretation. However, this results in high counting rates during blood-pool phase (green region) and the potential for detector saturation. Actual threshold for detector saturation will vary with scanner performance.

The simplified retention model can be considered as a special case of the 1-tissue-compartment model (neglecting the effects of tracer washout), in which case MBF must be estimated using the assumed tracer retention fraction (RF), together with the late-phase tissue activity (retention) measured after the first-pass transit (retention/RF = MBF). As shown in Figure 1, the extraction and retention fractions for ^{82}Rb are fairly similar, whereas the extraction of ^{13}N-ammonia is much higher (near unity) than the myocardial retention. The effects of tracer extraction, washout, and retention on image contrast in abnormally perfused myocardium (defects) are illustrated in Figure 2. A further simplification has been proposed to measure an index of stress–rest MFR using ^{18}F-flurpiridaz SUVs only (*14*). SUVs are unitless and measured simply as the late-phase myocardial activity divided by the total injected dose/kg of body weight. This method still requires additional validation but could simplify the stress–rest protocols substantially by removing the need for first-pass transit imaging and tracer kinetic modeling analysis.

Under resting conditions, autoregulation of myocardial tissue perfusion occurs in response to local metabolic demands. Resting MBF has been shown to vary linearly according to the product of heart rate and systolic blood pressure (*21*). Adjustment of resting MBF to account for changes in the heart rate–pressure product (RPP) should be considered as part of the interpretation of stress–rest MFR values, which can otherwise appear abnormal despite adequate stress MBF. Adjusted values are computed as $MBF_{ADJ} = MBF_{REST}/RPP_{REST} \times RPP_{REF}$, where RPP_{REF} is a reference value such as 8,500 reported for a typical CAD population (discussed in detail in the "Resting MBF" section) (*22*). Interpretation of the stress MBF together with the MFR is a complementary method to account for the confounding effects of resting hemodynamics on measured MFR (*23*).

To ensure accurate estimates of MBF and MFR, it is critical to verify that each dynamic series is acquired and analyzed correctly, with thorough review of quality assurance information as illustrated in Figure 4. Dynamic time–activity curves must include at least one background (zero-value) frame to ensure adequate sampling of the complete arterial blood input function. Assessment and correction of patient motion between the first-pass transit phase and the late-phase myocardial retention images are essential, as this can otherwise introduce a large bias in the estimated MBF values (*24*). The peak height of blood pool time–activity curves at rest and stress should be comparable (or slightly lower at stress) if similar radiotracer activities are injected. If there are substantial differences, extravasation or incomplete delivery of tracer may have occurred and may result in inaccurate MBF estimates (Fig. 5). The shape of the blood input function should also be standardized as much as possible (e.g., 30-s square wave), as variations in tracer injection profile have been shown to adversely affect MBF accuracy (*25*) and test–retest repeatability, in particular when using the simplified retention model (*26*). Blood pool

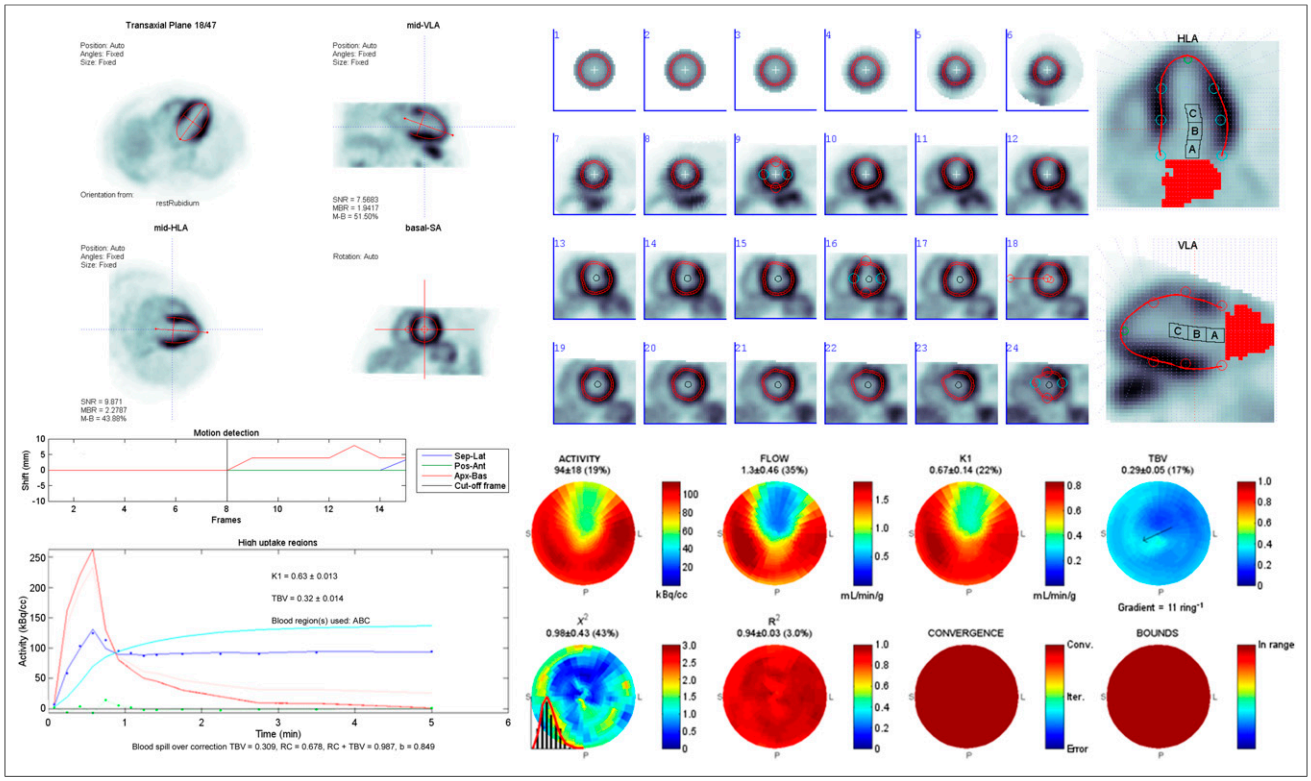

FIGURE 4. Example ^{82}Rb stress PET study quality assurance for PET quantification of MBF, including orientation of left ventricular long axis (A), sampling of myocardium and arterial blood regions (B), motion detection, dynamic time–activity curves and kinetic modeling curve-fit (C), regional MBF (FLOW) and total blood volume (TBV) maps, as well as χ^2 and R^2 goodness-of-fit metrics (D).

time–activity curves should also be visually examined for multiple peaks or broad peaks, which may suggest poor-quality injections due to poor-quality intravenous catheters, arm positioning, or other factors. Goodness-of-fit metrics such as residual χ^2 and coefficient of determination, R^2, should be consistently low and high, respectively. Standardization of software analysis methods has been reported for ^{13}N-ammonia (*27*) and ^{82}Rb (*28–30*), but significant variation remains among some vendor programs. Further standardization of image acquisition and analysis methods will have the benefit of allowing reliable pooling of MBF data as part of large, multicenter clinical trials.

Key Points

- Accurate and reproducible quantification of MBF is possible with both ^{13}N-ammonia and ^{82}Rb (both of which are Food and Drug Administration–approved).
- Consistent tracer injection profiles improve the reproducibility of MBF measurements.
- The administered dose must be adjusted to avoid detector saturation during the blood pool phase, which can be particularly challenging with ^{82}Rb.
- List-mode acquisition enables reconstruction of static, gated, and dynamic datasets. Dynamic datasets are used for blood flow quantification with compartmental modeling.

PROTOCOLS

Planning or Protocoling

This important step optimizes image quality, diagnostic accuracy, and safety. A personalized protocol for each patient considers the clinical history, reason for the test, patient preferences, and contraindications for stress agent. Reproducibility of the stress agent is critical for quantitative MBF studies to evaluate disease progression or response to therapy and requires the same stress agent, radiotracer, and software program.

Stress Test Procedure

The choice of hyperemic stress protocol is an important consideration for measurement and interpretation of MFR. Pharmacologic stress is generally required for MBF imaging because dynamic first-pass images must be acquired with the patient on the scanner bed. Although exercise stress may be preferred in some patients because of the added prognostic value of exercise capacity and electrocardiographic changes, the measured increase in rest-to-stress MBF is generally lower with exercise than with pharmacologic stress using adenosine, regadenoson, or dipyridamole. Exercise stress also reduces uptake by and spillover from adjacent organs such as the stomach and thus could reduce a potential source of artifact from MBF measurements. The use of supine bicycle exercise MBF imaging has been reported, but some detrimental effects of patient body motion may be expected. Further, this approach may be difficult to implement with the current generation of PET/CT scanners with longer imaging gantries.

Patient preparation for pharmacologic stress with PET is the same as for ^{99m}Tc SPECT MPI (*31*). Patients fast for a minimum of 4 h, avoid smoking for at least 4 h, and avoid caffeine intake for at least 12 h before vasodilator stress (*32–34*). Vasodilator stress with adenosine (*35*), dipyridamole (*36*), and regadenoson (*37*) has been evaluated using ^{13}N-ammonia, ^{82}Rb-chloride, and ^{15}O-water. After excluding contraindications, a stress agent is infused on the basis of standard protocols (Table 2). The timing

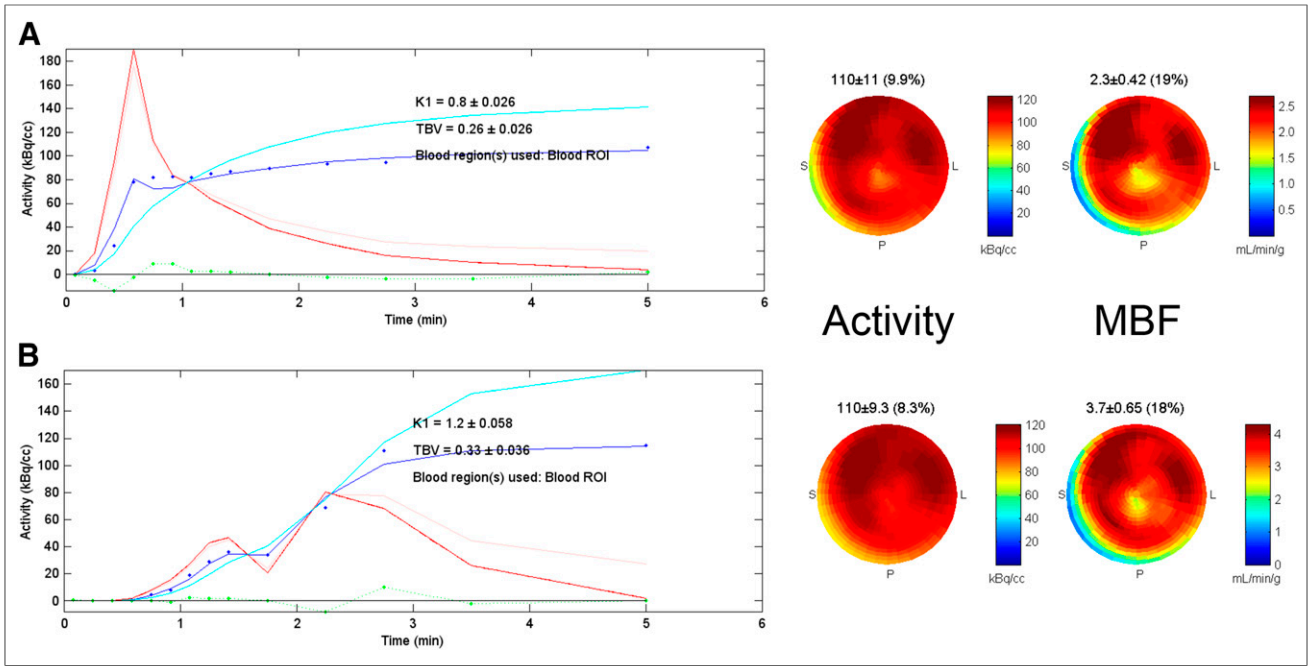

FIGURE 5. Test–retest dynamic ^{82}Rb PET MBF scans acquired at 3 and 13 min after dipyridamole stress. Typical injection profile (A) is shown with single peak of blood input curve (red) at ~30 s after scan start time. Poor-quality injection profile (B) shows delayed rise and double-peak of blood input curve, suggesting partial obstruction of intravenous line during tracer administration. Tracer uptake curves (dark blue) and polar maps (activity) are similar after 3–6 min, suggesting that full ^{82}Rb dose was eventually delivered. However, inconsistent curve shapes result in markedly different MBF estimates (3.7 vs. 2.3 mL/min/g), as derived from blood-pool-spillover– and partial-volume–corrected tissue curves (cyan).

of isotope injection varies for each stress agent. There is no advantage to using modified protocols such as high-dose dipyridamole or hand grip (attenuated hyperemic MBF) during dipyridamole stress and MBF imaging with PET (*38*). If vasodilator stress is contraindicated, dobutamine combined with atropine stress is an alternate and provides maximal hyperemia equivalent to that with dipyridamole (*39–41*), although there are some data indicating the contrary (*42–44*). Hyperemia from pharmacologic stress may be reversed for significant ischemic electrocardiography changes or symptoms about 3–4 min after the start of imaging, without jeopardizing quantitative MBF information.

TABLE 2
Stress Pharmaceuticals Used in PET MPI

Agent	Dose and administration	Timing of radiotracer injection	Route of radiotracer administration
Adenosine	140 mg/kg/min intravenous infusion for 4–6 min	Mid infusion	Two intravenous lines are preferred to prevent mid-infusion interruption of adenosine
Dipyridamole	0.56 mg/kg intravenous infusion over 4 min	3–5 min after completion of infusion	Single intravenous line for both stress agent and radioisotope
Regadenoson	0.4-mg rapid intravenous bolus (over 10 s)	Immediately after 10-mL saline flush*	Single intravenous line for both stress agent and radioisotope
Dobutamine	Stepwise increase in infusion from 5 or 10 μg/kg/min up to 40 μg/kg/min to achieve >85% predicted heart rate; atropine boluses may be used to augment heart rate response	Once target heart rate is achieved; continue dobutamine infusion for 1–2 min after radiotracer injection	Single intravenous line for both stress agent and radioisotope

*One recent study has suggested that injection of ^{82}Rb at 55 s, compared with 10 s, after injection of regadenoson resulted in greater maximal hyperemic MBF (2.33 ± 0.57 vs. 1.79 ± 0.44 mL/min/g) and correlated better with hyperemic MBF with dipyridamole (2.27 ± 0.57 mL/min/g) (*211*).

TABLE 3
MBF and MFR Reference Ranges for ^{13}N-Ammonia PET

Publication	Sample size (*n*)	Age (y)	Stress agent	Rest MBF (mL/min/g)	Stress MBF (mL/min/g)	MFR
Hutchins et al. (*212*)	7	24 ± 4	Dipyridamole	0.88 ± 0.17	4.17 ± 1.12	4.80 ± 1.30
Chan et al. (*213*)	20	35 ± 16	Dipyridamole	1.10 ± 0.20	4.33 ± 1.30	4.00 ± 1.30
Czernin et al. (*67*)	18	31 ± 9	Dipyridamole	0.76 ± 0.25	3.00 ± 0.80	4.1 ± 0.90
Czernin et al. (*38*)	11	27 ± 7	Dipyridamole	NR	2.13 ± 0.28	NR
Nagamachi et al. (*21*)	30	33 ± 15	Dipyridamole/adenosine	0.62 ± 0.14	2.01 ± 0.39	NR
Yokoyama et al. (*163*)	14	56 ± 10	Dipyridamole	0.70 ± 0.17	2.86 ± 1.20	4.13 ± 1.38
Böttcher et al. (*214*)	10	24 ± 5	Dipyridamole	0.61 ± 0.09	1.86 ± 0.27	3.16 ± 0.80
Campisi et al. (*215*)	10	62 ± 6	Dipyridamole	0.68 ± 0.16	2.04 ± 0.30	3.16 ± 0.85
Nitzsche et al. (*216*)	15	28 ± 12	Adenosine	0.64 ± 0.09	2.63 ± 0.75	NR
Dayanikli et al. (*159*)	11	48 ± 8	Adenosine	0.68 ± 0.80	2.64 ± 0.39	4.27 ± 0.52
Sawada et al. (*73*)	6	36 ± 14	Adenosine	0.71 ± 0.12	2.49 ± 0.74	3.50 ± 0.69
Beanlands et al. (*86*)	5	27 ± 4	Adenosine	0.62 ± 0.09	2.51 ± 0.27	4.10 ± 0.71
Muzik et al. (*217*)	10	26 ± 6	Adenosine	0.77 ± 0.16	3.40 ± 0.57	4.60 ± 0.90
Muzik et al. (*88*)	20	44 ± 11	Adenosine	0.67 ± 0.11	2.85 ± 0.49	4.28 ± 0.65
Lortie et al. (*22*)	14	NR	Dipyridamole	0.69 ± 0.09	2.71 ± 0.50	4.25 ± 0.91
DeGrado et al. (*218*)	8	NR	Dipyridamole	0.76 ± 0.17	2.68 ± 0.75	3.61 ± 1.06
Tawakol et al. (*71*)	7	NR	Adenosine	0.70 ± 0.19	3.51 ± 0.84	NR
Schindler et al. (*219*)	21	37 ± 13	Dipyridamole	0.61 ± 0.12	2.04 ± 0.37	NR
Quercioli et al. (*70*)	21	43 ± 11	Dipyridamole	0.71 ± 0.10	2.37 ± 0.49	3.38 ± 0.67
Valenta et al. (*220*)	26	38 ± 10	Dipyridamole	0.71 ± 0.13	2.29 ± 0.51	3.28 ± 0.70
Prior et al. (*68*)	50	42 ± 13	Dipyridamole/adenosine	0.64 ± 0.12	1.98 ± 0.44	3.40 ± 1.00
Renaud et al. (*221*)	14	31 ± 6	Dipyridamole	0.68 ± 0.12	2.86 ± 1.14	4.15 ± 1.57
Slomka et al. (*27*)	15	NR	Adenosine	0.85 ± 0.16	2.77 ± 0.65	3.39 ± 1.22
Weighted mean	363 (total)	37.6		0.71	2.58	3.54

NR = not reported.

Imaging Protocols

Typically, rest imaging is followed by stress imaging on the same day. Stress-first or stress-only imaging is feasible, but it is not routine practice with quantitative PET. Although several studies have suggested that peak hyperemic MBF is superior to MFR (*45–47*), most studies have concluded that MFR is more powerful for risk stratification (*48–53*), perhaps because of decreased variability compared with peak hyperemic MBF (*54*). Whether postischemic stunning affects resting MBF with stress-first imaging has not been well studied. Importantly, if regadenoson is used, reversal with 150 mg of aminophylline may not be sufficient to restore resting perfusion conditions (*55*). More data are needed before a transition to routine stress-only imaging for quantitative PET MBF imaging can be recommended.

Radiotracer Protocols

Table 1 lists doses of clinically used PET radiotracers for MBF imaging. The "Perfusion Tracers" section covers radiotracer properties in greater detail. Adjustment of injected activity for patient weight, body mass index, or attenuation is preferable to optimize trade-offs between the quality of delayed images and the potential for detector saturation with 3D PET. Use of automatic injectors will facilitate uniform delivery of the radiotracer and standardize the input function for MBF quantitation. Consistent tracer injection profiles may have advantages for reliable quantification of MBF (*26*), although additional clinical data will be helpful (*25*).

Image Acquisition and Reconstruction Parameters

Images are acquired and reconstructed using standard vendor-specific parameters. Briefly, after low-dose CT or a radionuclide localizing scan to position the heart, a dynamic or preferably list-mode acquisition is obtained in 2D or 3D mode. List-mode acquisition provides comprehensive data for static images, gated images for left ventricular volumes and ejection fraction, and dynamic images for MBF quantitation. It is important to keep the patient positioned consistently between the transmission and emission scans. Misalignment of the attenuation CT and PET emission images, potentially exacerbated by patient and respiratory motion during hyperemic stress, may introduce moderate to severe artifacts (*56*) in as many as 1 in 4 studies and can result in significant changes in MBF quantification (*57*). Camera vendors offer software to manually confirm and adjust alignment of the retention-phase PET images with the attenuation CT scan during image reconstruction. However, patient motion during the first-pass transit can produce inconsistent alignment of the dynamic image series, leading to attenuation artifacts and

TABLE 4
MBF and MFR Reference Ranges for ^{82}Rb PET

Publication	Sample size (*n*)	Age (y)	Stress agent	Rest MBF (mL/min/g)	Stress MBF (mL/min/g)	MFR
Lin et al. (*222*)	11	NR	Dipyridamole	1.15 ± 0.46	2.50 ± 0.54	NR
Lortie et al. (*22*)	14	NR	Dipyridamole	0.69 ± 0.14	2.83 ± 0.81	4.25 ± 1.37
Manabe et al. (*223*)	15	29 ± 9	Adenosine triphosphate	0.77 ± 0.25	3.35 ± 1.37	4.47 ± 1.47
Prior, et al. (*224*)	22	30 ± 13	Adenosine	1.03 ± 0.42	3.82 ± 1.21	3.88 ± 0.91
Sdringola et al. (*225*)	56	30 ± 13	Dipyridamole	0.72 ± 0.17	2.89 ± 0.50	4.17 ± 0.80
Johnson et al. (*171*)	241	28 ± 5	Dipyridamole	0.70 ± 0.15	2.71 ± 0.58	4.02 ± 0.85
Germino et al. (*226*)	9	28 ± 6	Regadenoson	0.92 ± 0.19	3.65 ± 0.64	NR
Renaud et al. (*221*)	14	31 ± 6	Dipyridamole	0.73 ± 0.15	2.96 ± 0.89	4.32 ± 1.39
Weighted mean	382 (total)	28.6		0.74	2.86	4.07

NR = not reported.

severe bias in MBF (*24*). Differences in reconstruction methods may have a substantial impact on measured MBF (*58*), and standardization is critical. Iterative reconstruction per manufacturer recommendations is preferred for dynamic image series. Minimal smoothing of the images is preferred for MBF quantitation.

Key Points

- To estimate MFR, maximal hyperemia is usually induced with dipyridamole, adenosine, or regadenoson.
- Typical imaging protocols for quantitative PET imaging involve rest imaging followed by stress imaging on the same day, although stress-only protocols may have a role.
- Quality control of dynamic images and time–activity curves is essential and should include inspection for emission–transmission misregistration, patient motion, and evidence of detector saturation.

PREFERRED NOMENCLATURE AND PHYSIOLOGIC REFERENCE RANGES

Nomenclature

A variety of terms have been used in the quantitative PET literature, including *coronary flow reserve* (*CFR*), *MFR, MBF reserve,* and *myocardial perfusion reserve.* Additionally, in the invasive and echocardiography literature, *coronary flow velocity reserve* is used. Finally, relative quantification of increased perfusion, without formal quantification of underlying MBF at rest and stress, has been referred to as *myocardial perfusion reserve index* in the cardiac MRI literature and has more recently been applied to quantification of SPECT images. The use of many different terms in the literature has the potential for confusion. Going forward and for this document, the preferred nomenclature is to refer to quantitative measures at rest or stress as *MBF* and the ratio of stress/rest MBF as *MFR*. Although this value generally correlates well with invasively determined CFR (*59–64*), PET methods do not measure volume of blood flow in the epicardial coronary arteries directly but rather blood flow in myocardial tissue. Thus, the term *MFR* is more appropriate. The standard units of MBF are milliliters·minute^{-1}·gram^{-1}, most commonly denoted as mL/min/g.

Resting MBF

Resting MBF as measured with PET and various positron-flow radiotracers has been reported to range from 0.4 to 1.2 mL/min/g (*65–71*). Apart from methodologic differences in radiotracer characteristics, tracer kinetic models, and image analysis that may introduce some variations between different studies, the variability of the reported resting MBF values may be attributed in part to differences in myocardial workload and thus the myocardial oxygen demand of the left ventricle (*66,67,72–74*). Sex and genetic variations, including mitochondrial function, are also important determinants contributing to the variability in resting MBF values (*75*).

MBF at rest and during some forms of stress is physiologically coupled with myocardial oxygen demand and thus correlates with indices of myocardial workload (e.g., rate–pressure product, defined as the product of systolic blood pressure and heart rate) (*76–78*). Consequently, resting MBF is commonly higher in patients with higher arterial blood pressure or heart rate (*67,70,79,80*). Age-related increases in resting MBF can be explained by rate–pressure product correction of increased systolic blood pressures (*67,81*). Most of the reported PET-determined resting MBF values have been higher in women than in men (*66,68,82,83*). Although the causes of this sex difference are not completely defined, hormonal effects on coronary circulatory function in women with CAD, and sex-dependent lipid profile changes, may be important contributors (*66,68,82,83*). Finally, in individuals with advanced obesity, resting MBF may also be elevated as induced by a more enhanced activation of the sympathetic nervous system and the renin–angiotensin–aldosterone axis, resulting in higher resting heart rate and arterial blood pressure (*70,83,84*).

Physiologic Ranges for MBF and MFR with ^{13}N-Ammonia and ^{82}Rb-Chloride

In 23 studies involving a total of 363 healthy subjects undergoing ^{13}N-ammonia PET, the weighted mean MBF values at rest and stress were 0.71 mL/min/g (range, 0.61–1.1) and 2.58 mL/g/min (range, 1.86–4.33), respectively (Table 3). Weighted mean MFR was 3.54 (range, 3.16–4.8). The corresponding values for 382 healthy subjects from 8 studies using ^{82}Rb PET are a weighted mean resting MBF of 0.74 mL/g/min (range, 0.69–1.15), a weighted

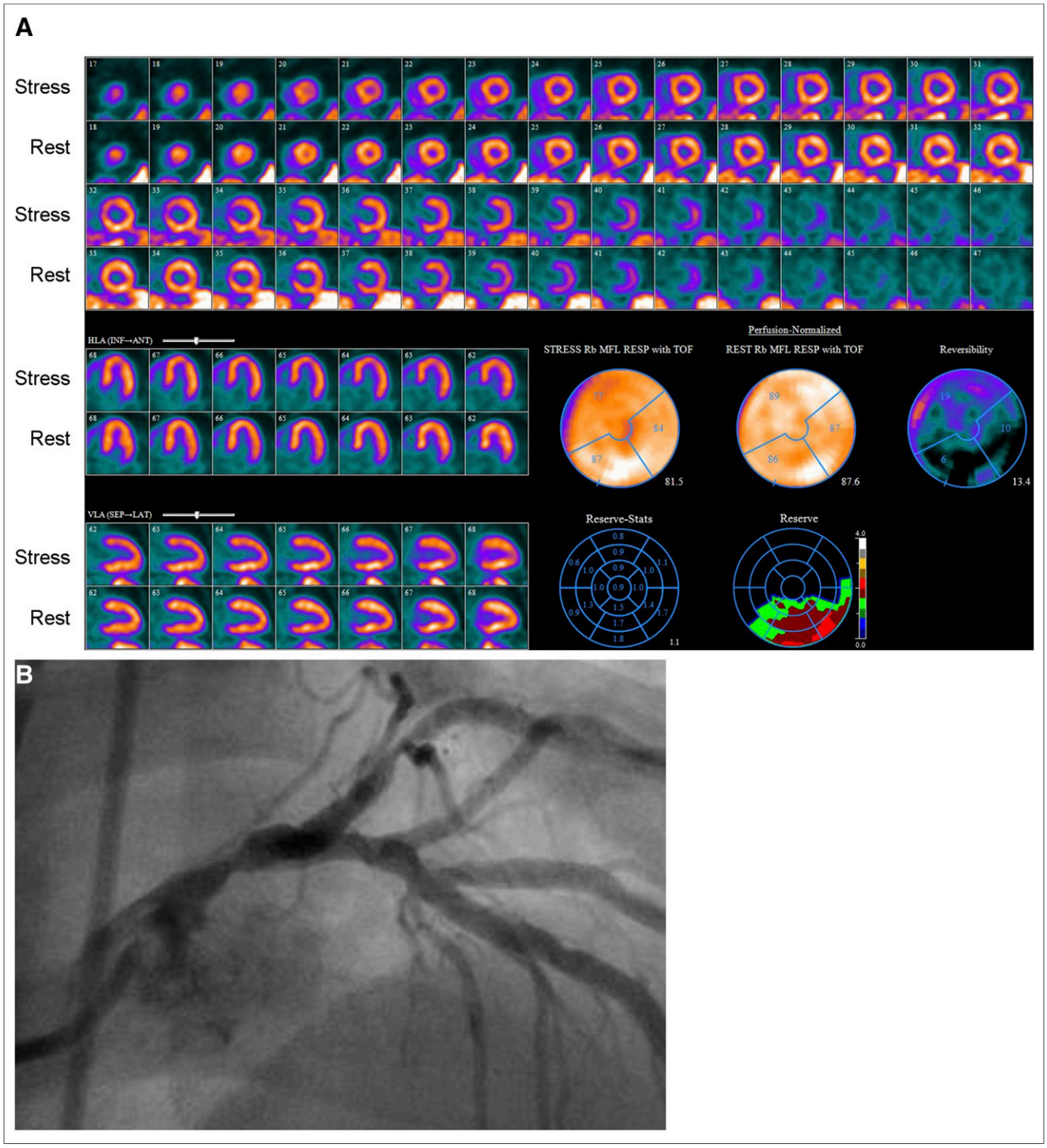

FIGURE 6. Clinical utility of blood flow quantification. In this example, from 81-y-old man with hypertension and dyslipidemia, relative MPI (A) with ^{82}Rb PET demonstrated only mild, reversible perfusion abnormality involving distribution of left anterior descending coronary artery. However, MFR was severely reduced globally at 1.11. Nearly entire heart had severely reduced MFR except for inferior and inferolateral walls, where it was only moderately reduced. Coronary angiography (B) showed severe stenosis of mid portion of left main coronary artery.

mean stress MBF of 2.86 mL/g/min (range, 2.5–3.82), and a weighted mean MFR of 4.07 (range, 3.88–4.47) (Table 4). It is critical to realize that these values represent physiologic ranges derived from young, healthy volunteers without coronary risk factors. In clinical populations, which are generally older and have a substantial burden of coronary risk factors, values below these ranges may frequently be seen and may not represent obstructive epicardial CAD. Instead, modest reductions in stress MBF or MFR below these reference ranges are often due to the effects of diffuse CAD and microvascular disease. A detailed discussion of abnormal thresholds for reporting and clinical action is found in the "Interpretation and Reporting" section.

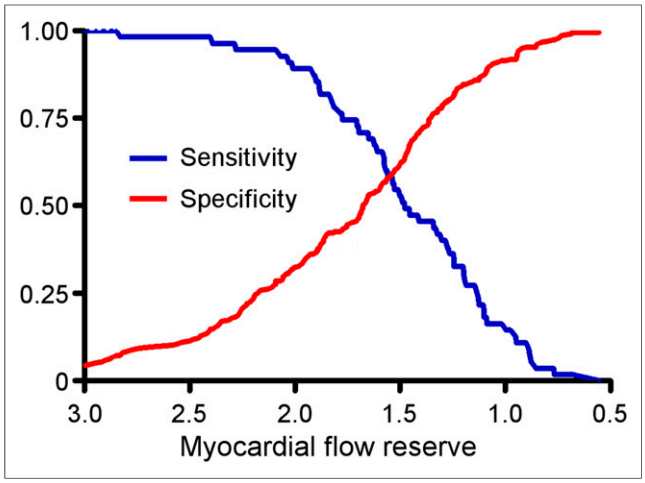

FIGURE 7. Receiver-operator characteristic curves for detection of severe CAD using MFR. As the threshold for abnormal MFR is decreased from 3.0 to 0.5, sensitivity for high-risk CAD (2-vessel disease including proximal left anterior descending artery, 3-vessel disease, and left main coronary artery) decreases (blue line). Conversely, with lower thresholds for defining abnormal MFR, specificity progressively increases (red line). (Adapted from Naya et al. (*91*).)

Key Points

- Although many terms have been used, *MBF* and *MFR* are the preferred terms for describing quantitative measures of blood flow.
- Physiologic reference ranges for rest and stress MBF and MFR vary by tracer and may be slightly higher for ^{82}Rb than for ^{13}N-ammonia.

INDICATIONS AND APPLICATIONS

CAD Diagnosis

A relationship between the severity of epicardial coronary artery stenoses and PET measures of both peak hyperemic stress MBF and MFR has been established for more than 2 decades (*85*). Though initially established using ^{15}O-water, this finding was quickly replicated using ^{13}N-ammonia (*86–88*) and more recently using ^{82}Rb (*89,90*). The application of stress MBF and MFR for improving the diagnostic accuracy of PET MPI with clinical protocols has been investigated by many groups with both ^{13}N-ammonia (*47,48,88*) and ^{82}Rb (*52,91*). Although these studies have consistently demonstrated improved diagnostic sensitivity (case example in Fig. 6), at least 2 large studies have raised concerns about potential for decreased specificity (Fig. 7) (*52,91*), possibly due to the contributions of diffuse atherosclerosis and microvascular disease to stress MBF and MFR measurements. Consequently, the positive predictive value of even severely depressed MFR (<1.5) is only modest (*52,91*). Conversely, preserved MFR (>2.0) has an excellent negative predictive value for high-risk CAD (i.e., left main and 3-vessel disease), and high-risk disease is extremely uncommon with an MFR of more than 2.5 (*52,91*) (see the "Interpretation and Reporting" section 6 for a more detailed discussion).

Prognostic Assessment

The incremental prognostic value of PET measures of stress MBF and MFR in patients with known or suspected CAD referred for clinical stress testing has also been extensively evaluated (Table 5) (*46,49,50,53,92–94*). Consistently, patients with more severely reduced stress MBF and MFR are at higher risk than patients with preserved values or modest reductions. An analysis of the relationship between MFR and cardiac mortality suggests an excellent prognosis for an MFR of more than 2 and a steady increase in cardiac mortality for an MFR of less than 2 (Fig. 8) (*54*). The largest of these studies has demonstrated that as many as half of intermediate-risk subjects may be reclassified on the basis of MFR, even after accounting for clinical characteristics, relative MPI interpretation, and left ventricular ejection fraction (*95*). Consequently, in patients at higher clinical risk, for whom even a low-risk relative assessment of MPI may be insufficiently reassuring (i.e., those likely to remain at intermediate posttest risk), referral for stress PET with quantification of MBF may be preferable as an initial test over relative MPI alone, such as with SPECT imaging.

Treatment Guidance

At present there are no randomized data supporting the use of any stress imaging modality for selection of patients for revascularization or for guidance of medical therapy. Observational data have established a paradigm that patients with greater degrees of ischemia on relative MPI are more likely to benefit from revascularization (*96*). This paradigm has been conceptually extended to include MFR and stress MBF (*97*) but has not yet been evaluated prospectively. Although observational data are limited to one single-center study with relatively small sample sizes, there is some evidence that early revascularization is associated with a more favorable prognosis only in patients with a low global MFR and that patients with a low MFR may benefit more from coronary artery bypass grafting than from percutaneous revascularization (*98*).

Special Populations

Diabetes Mellitus. Patients with diabetes mellitus are at significantly increased risk of CAD and its complications (*99*). Furthermore, diabetic patients may have extensive, high-risk CAD even with low-risk relative MPI findings (*100*), and diabetic patients with low-risk relative MPI findings may still be at significantly elevated risk of CAD complications (*101*). Important contributors to these concerning findings may be increased rates of diffuse epicardial CAD and microvascular disease among diabetic patients. Consequently, the improved performance of quantitative measures with PET compared with relative MPI is likely to be of particular value. In a large series of 1,172 patients with diabetes compared with 1,611 patients without diabetes, incorporation of MFR into PET assessment allowed identification of the 40% of diabetic patients who were at high risk (at equivalent risk to those with clinically recognized CAD) compared with the remainder, who experienced event rates comparable to individuals without diabetes (*102*). Given the important limitations of relative MPI among diabetic patients, PET with quantification of blood flow is preferable to SPECT among patients with diabetes mellitus.

Chronic Kidney Disease. Cardiovascular disease is the leading cause of death among patients with moderate to severe renal dysfunction (*103*), and early referral for revascularization may be beneficial in patients with suitable disease (*104*). However, patients with underlying renal dysfunction are also at increased risk of complications after angiography and revascularization (*105–107*). Unfortunately, as with diabetic patients, traditional relative

TABLE 5
Clinical Studies of Prognostic Value of Quantitative PET Blood Flow Estimates

Study	Subjects (*n*)	Population	Follow-up duration (y)	Primary endpoint	Radiotracer	Adjusted covariates	Hazard ratio
Herzog et al. (*49*)	256	Suspected myocardial ischemia	5.4	MACE	^{13}N-ammonia	Age, diabetes, smoking, abnormal perfusion (binary)	1.6 (MFR $<$ 2.0 vs. $\geq$ 2.0)
Tio et al. (*94*)	344	Ischemic heart disease	7.1	Cardiac death	^{13}N-ammonia	Age, sex	4.1 (per 0.5 MFR)
Slart et al. (*93*)	119	PET-driven revascularization	7.3	Cardiac death	^{13}N-ammonia	Age, sex	23.6 (MFR $<$ 1.34 vs. $>$ 1.67); 8.3 (MFR 1.34–1.67 vs. $>$ 1.67)
Murthy et al. (*50*)	2,783	Clinically indicated PET	1.4	Cardiac death	^{82}Rb	Age, sex, hypertension, dyslipidemia, diabetes, family history of premature CAD, tobacco use, history of CAD, body mass index, chest pain, dyspnea, early revascularization, rest LVEF, summed stress score, LVEF reserve	5.6 (MFR $<$ 1.5 vs. $>$ 2.0); 3.4 (MFR 1.5–2.0 vs. $>$ 2.0)
Fukushima et al. (*92*)	224	Clinically indicated PET	1.0	MACE	^{82}Rb	Age, summed stress score (dichotomized $>$ 4)	2.9 (MFR $<$ 2.11 vs. $\geq$ 2.11)
Ziadi et al. (*53*)	677	Clinically indicated PET	1.1	MACE	^{82}Rb	History of MI, stress LVEF, summed stress score (dichotomized $\geq$ 4)	3.3 (MFR $<$ 2.0 vs. $>$ 2.0)
Farhad et al. (*227*)	318	Suspected myocardial ischemia	1.7	MACE	^{82}Rb	Summed stress score	0.41 per mL/min/g stress MBF

MACE = major adverse cardiac events (cardiac death, nonfatal MI, late revascularization, cardiac hospitalization); LVEF = left ventricular ejection fraction; MI = myocardial infarction.

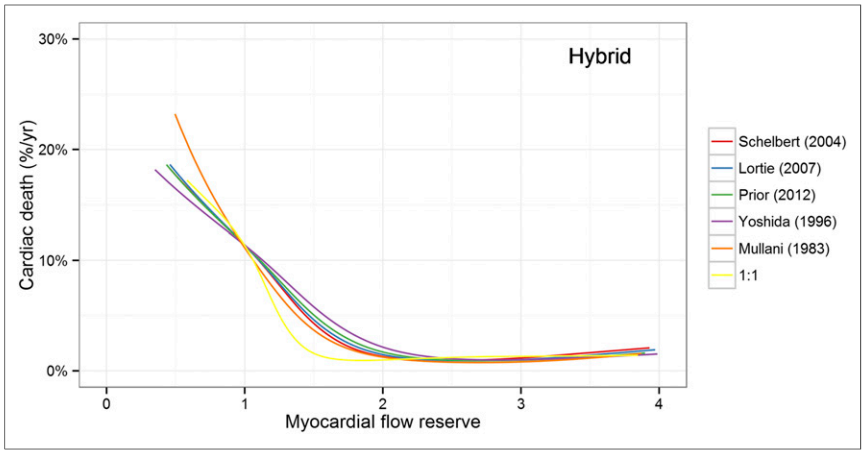

FIGURE 8. Relationship between MFR and risk of cardiac death. Regardless of which ^{82}Rb tracer kinetic model is used, similar pattern of rising risk with MFR < 2 is seen. 1:1 indicates fictitious 100% extraction (MBF = K_1), which approximates assumptions for myocardial perfusion reserve index. (Adapted from Murthy et al. (*54*).)

MPI is unable to identify truly low-risk patients (*108*). Two series from one center have shown that PET measures of MFR have greater prognostic value than do clinical and relative MPI parameters in patients with chronic kidney disease (*109*) and patients requiring renal replacement therapy (*110*).

Cardiomyopathy and Heart Failure. In many cases, relative MPI lacks sufficient negative predictive value to adequately rule out an ischemic etiology in patients with severe reductions in systolic function (*4*). However, patients with heart failure are also at increased risk of complications from invasive coronary angiography. Consequently, the excellent negative predictive value of preserved MFR may be of particular value in excluding severe multivessel CAD in patients with cardiomyopathy (*52,91*). Furthermore, in patients with both ischemic and nonischemic cardiomyopathies, impaired MFR is associated with markedly increased rates of major adverse cardiac events and cardiac death (*111*). However, it is important to note that abnormalities in MFR have been identified in cardiomyopathies of numerous etiologies (*112–116*). Consequently, whereas a low MFR does not necessarily imply an ischemic etiology, ischemic cardiomyopathy is extremely unlikely with well-preserved MFR. Nonetheless, the prognostic value of MFR is likely to be important regardless of etiology (*111,113,116*).

Heart Transplantation. Patients who have undergone heart transplantation may develop coronary allograft vasculopathy (CAV), a pathologic entity distinct from atherosclerotic CAD. In CAV, intimal fibromuscular hyperplasia and intimal–medial hyperplasia cause smooth narrowing of the coronary arteries with an attendant decrease in vasodilator capacity and MBF (*117,118*). Because arteries are usually smoothly narrowed, traditional noninvasive diagnostic techniques such as stress SPECT MPI and stress echocardiography may be limited compared with invasive imaging of the vessel wall using intravascular ultrasound or optical coherence tomography (*119–123*). Smooth narrowing of all vessels may result in normal relative MPI findings or only modest distal perfusion deficits despite global reductions in perfusion and vasodilator capacity. Invasive measures of MFR have been related to adverse outcomes (*124*). PET measures of MBF or MFR have been shown to correlate with invasive measures of CAV (*125*) and to identify patients at risk of developing CAV (*126*). Recently, a relatively large study of 140 patients with prior heart transplantation demonstrated that impaired MFR identified those at risk of developing clinical events (*127*). Indeed, investigational therapies for CAV have demonstrated an ability to improve PET measures of MFR (*128*). Of note, early after transplantation, decreases in MFR may not reflect early CAV (*129,130*), possibly because of resting hyperemia. In this early stage, stress MBF may have greater value. Despite this limitation, quantification of MBF in patients with prior heart transplantation has substantial well-established advantages over competing noninvasive methods of CAV diagnosis.

The Elderly. Older patients, by virtue of age alone, are at increased risk of mortality. However, among those of extremely advanced age, cancer rather than cardiovascular disease is the leading cause of mortality. Furthermore, whereas CAD is highly prevalent, the increased risks of invasive investigation and revascularization may shift the balance in some cases toward medical therapy rather than invasive approaches. One unpublished study has demonstrated that MFR assessment with PET may be able to identify patients aged 75 and older with excellent prognosis for survival free of cardiac death (*131*). Further investigation is of great interest.

Women. There is much debate in the literature (*132,133*) over optimal strategies for evaluation of known or suspected CAD in women. An important consideration is that a sizeable proportion of symptomatic women may have no evidence of obstructive CAD but are nonetheless at increased risk of cardiac complications (*134,135*). In part, this may be due more to impaired vasomotor function or microvascular disease than to epicardial obstructive stenoses in women compared with men (*136*). PET assessment of MFR has been demonstrated to be effective in both sexes and can readily identify evidence of epicardial obstructive disease, as well as diffuse CAD and microvascular function, noninvasively (*137*).

Chest Pain with Normal Findings on Coronary Angiography. In both men and women with CAD risk factors but without overt epicardial CAD, coronary vasomotor dysfunction is highly prevalent and can be identified with PET (*137*). This is likely due to the presence of diffuse disease and microvascular dysfunction and may be present even in the absence of coronary artery calcium (*138*). In one study of 901 patients referred for suspected CAD who had normal relative MPI results, patients with an MFR of less than 2 experienced a 5.2%/y rate of major adverse cardiac events, even with a coronary artery calcium score of zero. Consequently, assessment of MFR with PET has significant prognostic value even in patients believed to be at low risk on the basis of relative MPI.

Key Points

- Use of stress MBF and MFR for diagnosis is complex, as diabetes, hypertension, age, smoking, and other risk factors may decrease stress MBF and MFR without focal epicardial stenosis.
- Patients with preserved stress MBF and MFR are unlikely to have high-risk epicardial CAD.
- Severe reductions in global MFR (<1.5) are associated with a substantially increased risk of adverse outcomes and merit careful clinical consideration.

- A preserved global MFR of more than 2.0 has an excellent negative predictive value for high-risk CAD (i.e., left main and 3-vessel disease).

INTERPRETATION AND REPORTING

Reporting Quantitative MBF Data

One of the practical applications of measuring MBF and MFR with PET is the potential utility of these quantitative physiologic measures in improving the accuracy with which angiographic CAD is detected and its physiologic severity characterized, thereby allowing more informed decisions on referrals for cardiac catheterization and, potentially, revascularization. The decision on when and how to report MBF and MFR values in the context of MPI PET studies requires understanding of what is being measured, as well as the strengths and relative weaknesses of such physiologic parameters for clinical decision making.

The rationale for using quantitative MBF data for uncovering epicardial CAD is based on the relationship between peak hyperemic MBF and MFR and the severity of coronary lesions on coronary angiography demonstrated in experimental models of coronary stenosis (*139,140*) and in humans with atherosclerosis (*85–88*). The findings of human studies that have measured MBF and MFR noninvasively by PET, as well as angiographic stenosis severity, can be summarized as follows:

- In humans, resting MBF remains relatively preserved across a wide range of coronary stenosis severity (*85,86*), which is largely related to the gradual autoregulatory vasodilation of resistive vessels to maintain resting myocardial perfusion in the setting of upstream stenosis. Resting MBF falls only in the presence of critical subocclusive stenosis and poorly developed collateral blood flow.
- The activation of the compensatory autoregulatory changes described above results in a progressive loss in maximum vasodilator capacity with increasing stenosis severity, which is manifested by gradual reductions in hyperemic MBF and MFR as measured by PET (*85–87*).
- In general, hyperemic MBF and MFR are relatively preserved for coronary lesions with less than 70% angiographic stenosis or with preserved fractional flow reserve (FFR) (>0.8) (*45,47,51,52,85–89,91,141,142*). However, both may be reduced even in the absence of overt obstructive stenosis, especially in higher-risk subgroups (e.g., diabetes and prediabetic states (*143–154*), hypertension (*155–158*), dyslipidemia (*159–163*), and chronic kidney disease (*109,110,164,165*)).
- Hyperemic MBF and MFR are consistently reduced in lesions with greater than 70% luminal narrowing or those with abnormal FFR (*45,47,51,52,85–89,91,141,142*).
- Coronary stenosis of intermediate severity (e.g., 40%–90%) is associated with significant variability in hyperemic MBF and MFR. For any degree of luminal stenosis, the observed physiologic variability is likely multifactorial and includes the following: geometric factors of coronary lesions not accounted for by a simple measure of minimal luminal diameter, including shape, eccentricity, length, and entrance and exit angles, all of which are known to modulate coronary resistance (*166,167*); development of collateral blood flow (*166,167*); and presence of diffuse coronary atherosclerosis and microvascular dysfunction (combination of endothelial and smooth muscle cell dysfunction in resistive vessels, and microvascular rarefaction) (*168*), all of which are consistent findings in autopsy and intravascular ultrasound studies of patients with CAD (*169,170*).

Is there a physiologic threshold of hyperemic MBF or MFR that can be routinely used to accurately predict obstructive stenosis on coronary angiography? The simple answer is no. The available data from the published literature include a mix of patients with suspected or known CAD (e.g., prior myocardial infarction or percutaneous coronary intervention) and used different endpoints for defining lesion severity (e.g., visual or quantitative coronary stenosis severity, angiographic risk scores, or FFR) and methodologies for measuring MBF (e.g., ^{15}O-water, ^{13}N-ammonia, or ^{82}Rb using different quantitative approaches), resulting in multiple different thresholds being proposed to improve detection of obstructive angiographic CAD. Nonetheless, there are a few areas of agreement that have potentially important practical implications for including quantitative flow data in clinical PET MPI reports:

- A preserved global hyperemic MBF and MFR consistently reduce the probability of high-risk angiographic CAD (i.e., obstructive proximal stenosis in all 3 major coronary arteries, or left main disease). A global hyperemic MBF of more than 2 mL/min/g and MFR of more than 2 reliably exclude the presence of high-risk angiographic CAD (negative predictive value > 95%) (*51,52,91*).
- A severely reduced global hyperemic MBF and MFR identify patients at high risk for major adverse cardiovascular events, including death. Although thresholds may vary in different labs using different software, in general an MFR of less than 1.5 should be considered a high-risk feature on MPI PET (*46,49,50,53,92,94,98,102*) and is associated with an increased likelihood for multivessel obstructive CAD (*51,52,91*). In these patients, angiographic evaluation may be necessary to exclude disease that can potentially by revascularized (*98*).
- A severe reduction in hyperemic MBF (<1.5 mL/min/g) or MFR (<1.5) in a single vascular territory in a patient with normal MPI PET results by semiquantitative visual analysis should raise the possibility of flow-limiting CAD.

It is important to understand that these thresholds may vary in different labs using different software, and consequently, this should be viewed as a guide. Although individual labs may adopt variations of these thresholds, the general principle that coronary anatomy may need to be defined in patients with severely reduced MFR remains important.

Hyperemic MBF, MFR, or Both?

Hyperemic MBF and MFR provide useful information on coronary vasodilator flow capacity and characterization of flow-limiting CAD. Both parameters also share the same limitation for differentiating predominant focal obstructive stenosis from diffuse atherosclerosis and microvascular dysfunction. For most patients, the information from these two parameters is concordant (normal or abnormal) (*171*). However, in a minority of patients the information may be discordant. Since MFR is a ratio between hyperemic and resting MBF, unusually low or high resting MBF will affect MFR and result in discrepant findings compared with the hyperemic MBF value. For example, patients with prior myocardial infarction may show relatively preserved MFR in infarct-related territories because of low resting MBF. Conversely, patients with normal hyperemic MBF but unusually high resting MBF (e.g., women and heart transplant recipients) may show a

relatively reduced MFR. Consequently, both parameters should be considered in the interpretation of the test results.

In studies that have examined the incremental value of MBF quantification for predicting obstructive coronary stenosis on angiography, both hyperemic MBF and MFR have performed similarly (*45,47*). This suggests that stress-only imaging may be effective in selected patients, especially those without known CAD and normal left ventricular ejection fraction in whom resting MPI may be unnecessary to assess defect reversibility.

From a prognostic perspective, MFR provides better incremental risk stratification than hyperemic MBF alone (*50,53*). Furthermore, patients on medical therapies that reduce resting MBF, such as β-blockers, may have reduced hyperemic MBF due to disease but may be asymptomatic because of adequate MFR and thus not be in need of intervention (*10*), further justifying the need to measure both resting and hyperemic MBF to derive the MFR.

Complementary Role of Coronary CT Angiography

The addition of coronary CT angiography can be quite helpful to differentiate patients with extensive obstructive CAD from those with predominantly microvascular dysfunction (*172–176*). The addition of CT angiography information can improve the specificity of PET, especially in the setting of abnormal MBF values (*35*).

Special Considerations for Reporting MBF and MFR

MBF and MFR studies should be conducted and interpreted by experienced labs. The interpretation must consider the clinical context and the question being asked by the referring provider—for example, whether the question is specifically regarding myocardial ischemia, the hemodynamic significance of disease, microvascular disease, transplant vasculopathy, or some combination of these. The interpretation must also consider the findings of other imaging studies, including electrocardiography changes, coronary calcium score, and coronary anatomy (if CT angiography is performed), as well as high-risk features such as transient ischemic dilation, right ventricular uptake, and lack of augmentation of systolic function with stress.

The reporting physician needs to consider how the information will add value to the diagnostic information and potentially affect decision making so as not to lead to unnecessary testing or undertesting. Conditions known to be associated with diffuse atherosclerosis or microvascular dysfunction that would impair global MFR need to be considered, such as renal failure, prior bypass surgery, and global left ventricular dysfunction. As noted, conditions under which accurate measurement of MFR may not be possible, as in large regions of myocardial infarction, should also be considered. Because these conditions are often already associated with an increased risk of events, the added value of MBF and MFR measurements for prognostication may be limited under these circumstances (Table 6).

Special consideration must be made when there is no flow augmentation. Typically, there is some type of change even for severe MFR impairment, and the change is often heterogeneous; that is, some regions may decrease, suggesting steal, and some may increase. Likewise, such severe impairments are often accompanied by other findings, such as transient ischemic dilation, right ventricular uptake, electrocardiography changes, or regional ischemia on relative MPI. When these are not present, when perfusion appears normal, and when errors in stress-agent administration have been excluded—yet MFR is uniform at 1.0 or very close to 1.0—the possibility should be considered that the patient has ingested caffeine or is not responsive to vasodilator stress. The test may need to be repeated with a different stress agent such as dobutamine (Table 6) (*177,178*).

TABLE 6
Reporting MFR in Clinical Practice*

Report MFR any time MFR adds value toward diagnosis or stratification	Be cautious reporting MFR† when MFR provides no diagnostic or prognostic value, might confuse management, or might lead to unnecessary tests
Normal perfusion, high normal MFR	History of conditions known to impair long-term microvascular function
Abnormal perfusion with more severely or diffusely reduced MFR than expected	Chronic renal failure
Microvascular measurements specifically requested	Prior coronary artery bypass grafting
Assessment of hemodynamic significance of lesion specifically requested	Global left ventricular dysfunction (suspected cardiomyopathy)
	Accurate MFR measurement not possible or might be misleading
	Large prior myocardial infarction
	Suspected caffeine/methylxanthine ingestion

*Adapted from Juneau et al. (*178*).
†Depending on experience of lab and understanding of MBF and MFR concepts of referring provider, it may be appropriate to not report findings under these circumstances to avoid confusion and potentially unnecessary subsequent testing.

Key Points

- Preserved stress MBF of more than 2 mL/min/g and MFR of more than 2 reliably exclude the presence of high-risk angiographic disease (negative predictive value > 95%) and are reasonable to report when used in clinical interpretation.
- A severely decreased global MFR (<1.5 mL/min/g) should be reported as a high-risk feature for adverse cardiac events but is not always due to multivessel obstructive disease. The likelihood of multivessel obstructive disease may be refined by examination of the electrocardiogram, regional perfusion, coronary calcification, and cardiac volumes and function.
- Regional decreases in stress MBF (<1.5 mL/min/g) and MFR (<1.5) in a vascular territory may indicate regional flow-limiting disease.

PHYSIOLOGIC RELATIONSHIPS AMONG MFR, FFR, AND RELATIVE FLOW RESERVE

Traditionally, treatment decisions on medical therapy, percutaneous coronary intervention, or coronary artery bypass grafting have been based on the visual interpretation of the coronary

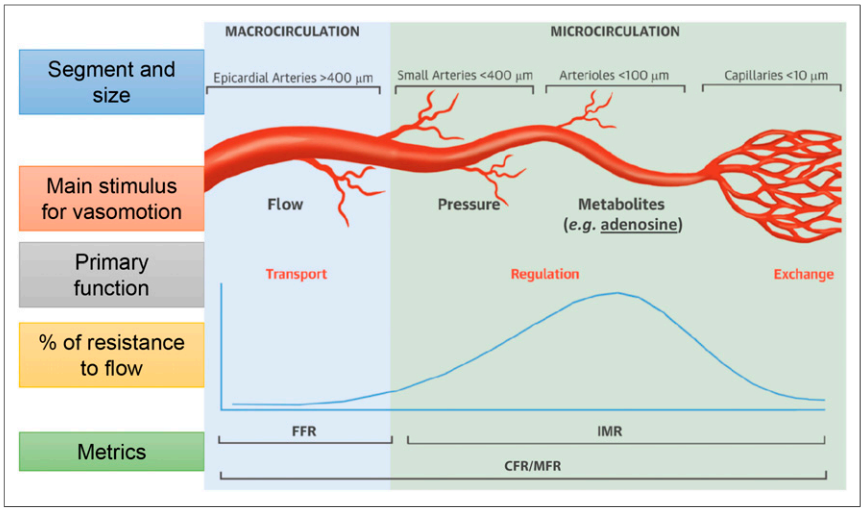

FIGURE 9. Comparison of physiologic basis of FFR and MFR. FFR is affected by focal stenosis and diffuse atherosclerosis of coronary macrocirculation, whereas index of microcirculatory resistance (IMR) reflects disease of smaller vessels. However, because intact arteriolar microcirculation is required for action of adenosine, FFR may be falsely reassuring in setting of microvascular dysfunction. MFR and CFR integrate entire coronary circulation. (Derived from De Bruyne et al. (*230*).)

angiogram, despite extensive evidence that subjective grading of luminal stenosis correlates poorly with hemodynamic significance—particularly for coronary stenoses between 30% and 80% of luminal diameter (*179–181*). Quantitative noninvasive and invasive techniques are now available that go beyond standard interpretation of anatomic coronary stenosis in making this functional assessment. These include noninvasive assessment of maximum MBF and MFR with PET, as well as invasive measurement of CFR and FFR. Noninvasive estimation of FFR using CT has also recently been described (*182*). Although both FFR and MFR can be used to assess the functional significance of stenosis, what they actually measure, their physiologic basis, and their clinical implications are distinct.

FFR

Invasive FFR has become a well-studied and increasingly used technique providing a surrogate measure of flow limitation and lesion-level ischemia. FFR assesses large-vessel coronary stenosis and is defined as the ratio of maximal blood flow in a stenotic artery relative to maximal flow in the same artery in the theoretic absence of any stenosis (Fig. 9) (*183–186*). FFR is calculated as the ratio of distal coronary pressure and aortic pressure, typically measured using an intracoronary pressure wire during adenosine-induced maximal hyperemia, based on the assumption that during maximal vasodilation, coronary resistance is negligible.

An FFR of less than 0.75 was originally shown to detect reversible ischemia, defined by noninvasive stress testing (thallium SPECT and PET, dobutamine stress echocardiography, or exercise stress testing), whereas an FFR of more than 0.8 excludes ischemia with a predictive value of over 95% (*184*). Randomized trials—including Fractional Flow Reserve versus Angiography for Multivessel Evaluation (FAME) and FAME-2, which used an FFR cutoff point of 0.8 (*187,188*)—have provided evidence that the use of FFR to guide clinical decisions on coronary revascularization results in reduced cardiac events. On the basis of these findings, the use of FFR is now incorporated into guidelines on management of patients with stable ischemic heart disease (*187–189*).

FFR, however, has multiple limitations (*190*). In the presence of serial stenoses, a distal lesion artificially reduces the pressure gradient across the proximal lesion, leading to an overestimation of the proximal lesion's ratio of distal coronary pressure to aortic pressure, thus underestimating its functional significance (*191,192*). Conversely, the presence of a proximal lesion artificially lowers this ratio for the distal lesion. Further, FFR assumes an intact microcirculation because this is the site of action of adenosine. FFR can appear falsely normal in the presence of microvascular dysfunction or disease, since elevated pressure distal to a critical stenosis, associated with increased resistance due to a microvascular abnormality, may result in a normal pressure drop across a hemodynamically significant lesion (*193,194*). Further, in the presence of diffuse atherosclerosis, FFR may be abnormal even without focal stenosis (*195*). Finally, in the setting of excellent flow capacity, the clinical significance of a reduced FFR across a moderate lesion may be overestimated if peak flow is still sufficient to meet myocardial oxygen demand. In this circumstance, symptoms are unlikely to improve with revascularization despite the reduced FFR.

More recently, the invasively measured instantaneous wave-free ratio has been advanced as a quantitative metric—which can be measured without use of a vasodilator—of the hemodynamic significance of a lesion. Although there has been only limited exploration of the relationships between the instantaneous wave-free ratio and MFR assessed by PET (*196*), inconsistencies between the instantaneous wave-free ratio and FFR are common (*197–199*). Nonetheless, two randomized trials have demonstrated that a strategy using an instantaneous wave-free ratio of more than 0.89 to defer revascularization yielded noninferior outcomes to a strategy using an FFR of more than 0.8 (*200,201*).

Assessments of MBF and Flow Reserve

Quantification of MBF using PET, allowing assessment of peak hyperemic MBF as well as noninvasive calculation of MFR, is physiologically distinct from FFR (*202*). Unlike FFR, MFR evaluates the effects of abnormality over the entire coronary circulation (Fig. 9). It therefore allows assessment not only of the effects of focal epicardial coronary stenosis but also of diffuse coronary atherosclerosis and microvascular dysfunction. As discussed above, an important clinical limitation of blood flow quantitation compared with FFR is that it is difficult to distinguish abnormality due to epicardial artery stenosis from that due to diffuse atherosclerosis, microcirculatory dysfunction, or both. Relative flow reserve—the ratio of stress MBF in regions subtended by stenotic arteries to stress MBF in regions subtended by nonstenotic arteries—has been proposed as one potential solution. However, as with relative assessments of stress perfusion defects by PET, computation of relative flow reserve requires an assumed or defined normal zone for comparison.

CFR can also be measured invasively on a per-territory basis at the time of cardiac catheterization, using an intracoronary wire that assesses flow velocity (*203*). For invasive CFR, each vessel must be assessed separately, with repeated runs of vasodilator for maximal hyperemia. Importantly, for assessments of coronary physiology during cardiac catheterization, FFR and CFR can now be measured simultaneously with combined pressure sensor– and flow sensor–tipped guidewires (*204*). More recently, quantitative estimates of myocardial perfusion from Doppler echocardiography (*205,206*) and contrast echocardiography (*207*) have emerged as having clinical value.

Discrepancies Between FFR and MFR

The different physiologic basis of FFR and MFR measurements explains how discrepancies between FFR and assessments of MBF and MFR may arise. FFR, a lesion-based index, assumes uniform endothelial function on either side of the lesion and an intact microcirculation, whereas MBF and MFR consider the entire vascular system of the heart as a totality (Fig. 9). Myocardial ischemia associated with diffuse coronary atherosclerosis or microvascular disease in the absence of significant epicardial stenosis will therefore affect MFR and FFR differently (*208*). Of note, a current multicenter randomized clinical trial—DEFINE-Flow (Distal Evaluation of Functional Performance with Intravascular Sensors to Assess the Narrowing Effect–Combined Pressure and Doppler Flow Velocity Measurements)—is assessing whether, in the presence of an invasive CFR of more than 2 and coronary lesions with an FFR of less than 0.80, percutaneous coronary intervention can be safely deferred (*209*). Estimates of the functional significance of coronary stenoses by FFR and the noninvasive or invasive CFR techniques usually agree. Concordantly normal studies imply the absence of hemodynamically significant epicardial or microvascular disease. Concordantly abnormal studies imply the presence of significant epicardial stenosis, with or without additional diffuse atherosclerotic or microvascular disease. However, a study by Johnson et al., assembling all combined invasive CFR and FFR measurements throughout the literature (a total of 438 cases), reported only a modest linear correlation between CFR and FFR ($r = 0.34$, $P < 0.001$), with 30%–40% of lesions showing discordance (*210*). Discordance is largely explained by the mechanisms discussed above. When the discordance is that low FFR is seen in regions with normal CFR, a flow decrement that is insufficient to cause ischemia may be the most likely cause, and percutaneous coronary intervention would be unlikely to improve symptoms. The discordance of low MFR with normal FFR is most commonly due to microvascular disease in the setting of diffuse nonobstructive epicardial disease or in isolation (*193,194*).

Thus, both FFR and MFR provide valuable physiologic information for patient management but assess different pathophysiologic processes. Knowledge of these differences is important in understanding the frequently observed discordance between these measurements. For invasive assessment, these considerations lend impetus to increasing the use of physiologic measurements and combining the results of FFR, MFR, and stenosis for a unified interpretation. For noninvasive testing, they point to the value of combining absolute quantitative and regional assessments of perfusion with anatomic assessment—using coronary artery calcification scans or angiography (either invasive or noninvasive)—in settings in which overall clinical assessment based on the physiologic approach alone is not definitive.

Key Points

- PET MFR/invasive CFR and invasive FFR are related but are not interchangeable measures, with discordance in 30%–40% of lesions.
- MFR and invasive CFR measure the combined hemodynamic effects of epicardial stenosis, diffuse disease, and microvascular dysfunction. FFR measures the combined hemodynamic effects of focal and diffuse atherosclerosis. Microvascular dysfunction increases coronary resistance and blunts the pressure gradient across a stenosis and may sometimes lead to falsely negative FFR readings of flow-limiting lesions. The latter may explain some of the discrepancies between FFR and MFR/CFR.

FUTURE CHALLENGES AND CONCLUSIONS

Quantification of MBF and MFR represents a substantial advance for diagnostic and prognostic evaluation of suspected or established CAD. These methods are at the cusp of translation to clinical practice. However, further efforts are necessary to standardize measures across laboratories, radiotracers, equipment, and software. Most critically, data are needed supporting improved clinical outcomes when treatment selection is based on these measures.

DISCLOSURE

Venkatesh Murthy owns stock in General Electric, Mallinckrodt Pharmaceuticals, and Cardinal Health and has received research funding from INVIA Medical Imaging Solutions and speaker honoraria from Bracco Diagnostics and Ionetix. Rob Beanlands has received research grants from General Electric, Lantheus Medical Imaging, and Jubilant Draximage and speaker honoraria from Lantheus Medical Imaging and Jubilant Draximage. Salvador Borges-Neto has received research grants, speaker honoraria, and consulting fees from General Electric. E. Gordon DePuey serves on the advisory board for Adenosine Therapeutics. Ernest Garcia receives royalties from the sale of the Emory Cardiac Toolbox. Terrence Ruddy has received research grants from General Electric HealthCare and Advanced Accelerator Applications. Piotr Slomka has received research grants from Siemens Healthcare and receives royalties from Cedars-Sinai Medical Center. Dan Berman receives royalties from Cedars-Sinai Medical Center. Edward Ficaro has an ownership interest in INVIA Medical Imaging Solutions. No other potential conflict of interest relevant to this article was reported.

REFERENCES

1. Bateman TM, Maddahi J, Gray RJ, et al. Diffuse slow washout of myocardial thallium-201: a new scintigraphic indicator of extensive coronary artery disease. *J Am Coll Cardiol.* 1984;4:55–64.
2. Lima RSL, Watson DD, Goode AR, et al. Incremental value of combined perfusion and function over perfusion alone by gated SPECT myocardial perfusion imaging for detection of severe three-vessel coronary artery disease. *J Am Coll Cardiol.* 2003;42:64–70.
3. Maddahi J, Garcia EV, Berman DS, Waxman A, Swan HJ, Forrester J. Improved noninvasive assessment of coronary artery disease by quantitative analysis of regional stress myocardial distribution and washout of thallium-201. *Circulation.* 1981;64:924–935.
4. Berman DS, Kang X, Slomka PJ, et al. Underestimation of extent of ischemia by gated SPECT myocardial perfusion imaging in patients with left main coronary artery disease. *J Nucl Cardiol.* 2007;14:521–528.
5. Watson DD, Glover DK. Overview of tracer kinetics and cellular mechanisms of uptake. In: Beller GA, Zaret BA, eds. *Clinical Nuclear Cardiology.* 4th ed. Philadelphia, PA: Mosby; 2010:3–13.

6. Shanoudy H, Raggi P, Beller GA, et al. Comparison of technetium-99m tetrofosmin and thallium-201 single-photon emission computed tomographic imaging for detection of myocardial perfusion defects in patients with coronary artery disease. *J Am Coll Cardiol.* 1998;31:331–337.
7. Soman P, Taillefer R, DePuey EG, Udelson JE, Lahiri A. Enhanced detection of reversible perfusion defects by Tc-99m sestamibi compared to Tc-99m tetrofosmin during vasodilator stress SPECT imaging in mild-to-moderate coronary artery disease. *J Am Coll Cardiol.* 2001;37:458–462.
8. Moody JB, Lee BC, Corbett JR, Ficaro EP, Murthy VL. Precision and accuracy of clinical quantification of myocardial blood flow by dynamic PET: a technical perspective. *J Nucl Cardiol.* 2015;22:935–951.
9. Murthy VL, Di Carli MF. Non-invasive quantification of coronary vascular dysfunction for diagnosis and management of coronary artery disease. *J Nucl Cardiol.* 2012;19:1060–1072.
10. Gould KL, Johnson NP, Bateman TM, et al. Anatomic versus physiologic assessment of coronary artery disease: role of coronary flow reserve, fractional flow reserve, and positron emission tomography imaging in revascularization decision-making. *J Am Coll Cardiol.* 2013;62:1639–1653.
11. CardioGen-82 Rubidium Rb 82 Generator [package insert]. Monroe Township, NJ: Bracco Diagnostics; April 2013.
12. RUBY-FILL (rubidium Rb 82 generator) [package insert]. Kirkland, Quebec, Canada: Jubilant DraxImage; November 2016.
13. Yu M, Guaraldi MT, Mistry M, et al. BMS-747158-02: a novel PET myocardial perfusion imaging agent. *J Nucl Cardiol.* 2007;14:789–798.
14. Sherif HM, Nekolla SG, Saraste A, et al. Simplified quantification of myocardial flow reserve with flurpiridaz F 18: validation with microspheres in a pig model. *J Nucl Med.* 2011;52:617–624.
15. Renaud JM, Yip K, Guimond J, et al. Characterization of 3-dimensional PET systems for accurate quantification of myocardial blood flow. *J Nucl Med.* 2017;58:103–109.
16. Keiding S, Sørensen M, Munk OL, Bender D. Human ^{13}N-ammonia PET studies: the importance of measuring ^{13}N-ammonia metabolites in blood. *Metab Brain Dis.* 2010;25:49–56.
17. Yoshida K, Mullani N, Gould KL. Coronary flow and flow reserve by PET simplified for clinical applications using rubidium-82 or nitrogen-13-ammonia. *J Nucl Med.* 1996;37:1701–1712.
18. Erthal L, Erthal F, Beanlands RSB, Ruddy TD, deKemp RA, Dwivedi G. False-positive stress PET-CT imaging in a patient with interstitial injection. *J Nucl Cardiol*. August 12, 2016 [Epub ahead of print].
19. Morris ED, Endres CJ, Schmidt KC, Christian BT, Muzic RF Jr, Fisher RE. Kinetic modeling in positron emission tomography. In: Wernick MN, Aarsvold JN, eds. *Emission Tomography.* San Diego, CA: Academic Press; 2004:499–540.
20. deKemp RA, Yoshinaga K, Beanlands RSB. Will 3-dimensional PET-CT enable the routine quantification of myocardial blood flow? *J Nucl Cardiol.* 2007;14:380–397.
21. Nagamachi S, Czernin J, Kim AS, et al. Reproducibility of measurements of regional resting and hyperemic myocardial blood flow assessed with PET. *J Nucl Med.* 1996;37:1626–1631.
22. Lortie M, Beanlands RSB, Yoshinaga K, Klein R, Dasilva JN, DeKemp RA. Quantification of myocardial blood flow with ^{82}Rb dynamic PET imaging. *Eur J Nucl Med Mol Imaging.* 2007;34:1765–1774.
23. Johnson NP, Gould KL. Physiological basis for angina and ST-segment change: PET-verified thresholds of quantitative stress myocardial perfusion and coronary flow reserve. *JACC Cardiovasc Imaging.* 2011;4:990–998.
24. Hunter CRRN, Klein R, Beanlands RS, deKemp RA. Patient motion effects on the quantification of regional myocardial blood flow with dynamic PET imaging. *Med Phys.* 2016;43:1829.
25. Raylman RR, Caraher JM, Hutchins GD. Sampling requirements for dynamic cardiac PET studies using image-derived input functions. *J Nucl Med.* 1993;34:440–447.
26. Klein R, Ocneanu A, Renaud JM, Ziadi MC, Beanlands RSB, deKemp RA. Consistent tracer administration profile improves test-retest repeatability of myocardial blood flow quantification with ^{82}Rb dynamic PET imaging. *J Nucl Cardiol*. November 1, 2016 [Epub ahead of print].
27. Slomka PJ, Alexanderson E, Jácome R, et al. Comparison of clinical tools for measurements of regional stress and rest myocardial blood flow assessed with ^{13}N-ammonia PET/CT. *J Nucl Med.* 2012;53:171–181.
28. Dekemp RA, Declerck J, Klein R, et al. Multisoftware reproducibility study of stress and rest myocardial blood flow assessed with 3D dynamic PET/CT and a 1-tissue-compartment model of ^{82}Rb kinetics. *J Nucl Med.* 2013;54:571–577.
29. Nesterov SV, Deshayes E, Sciagrà R, et al. Quantification of myocardial blood flow in absolute terms using ^{82}Rb PET imaging: the RUBY-10 study. *JACC Cardiovasc Imaging.* 2014;11:1119–1127.
30. Tahari AK, Lee A, Rajaram M, et al. Absolute myocardial flow quantification with ^{82}Rb PET/CT: comparison of different software packages and methods. *Eur J Nucl Med Mol Imaging.* 2014;41:126–135.
31. Henzlova MJ, Duvall WL, Einstein AJ, Travin MI, Verberne HJ. ASNC imaging guidelines for SPECT nuclear cardiology procedures: stress, protocols, and tracers. *J Nucl Cardiol.* 2016;23:606–639.
32. Böttcher M, Czernin J, Sun KT, Phelps ME, Schelbert HR. Effect of caffeine on myocardial blood flow at rest and during pharmacological vasodilation. *J Nucl Med.* 1995;36:2016–2021.
33. Kubo S, Tadamura E, Toyoda H, et al. Effect of caffeine intake on myocardial hyperemic flow induced by adenosine triphosphate and dipyridamole. *J Nucl Med.* 2004;45:730–738.
34. Lapeyre AC, Goraya TY, Johnston DL, Gibbons RJ. The impact of caffeine on vasodilator stress perfusion studies. *J Nucl Cardiol.* 2004;11:506–511.
35. Kajander S, Joutsiniemi E, Saraste M, et al. Cardiac positron emission tomography/computed tomography imaging accurately detects anatomically and functionally significant coronary artery disease. *Circulation.* 2010;122:603–613.
36. Al-Mallah MH, Sitek A, Moore SC, Di Carli M, Dorbala S. Assessment of myocardial perfusion and function with PET and PET/CT. *J Nucl Cardiol.* 2010;17:498–513.
37. Hsiao E, Ali B, Blankstein R, et al. Detection of obstructive coronary artery disease using regadenoson stress and ^{82}Rb PET/CT myocardial perfusion imaging. *J Nucl Med.* 2013;54:1748–1754.
38. Czernin J, Auerbach M, Sun KT, Phelps M, Schelbert HR. Effects of modified pharmacologic stress approaches on hyperemic myocardial blood flow. *J Nucl Med.* 1995;36:575–580.
39. Bartunek J, Wijns W, Heyndrickx GR, de Bruyne B. Effects of dobutamine on coronary stenosis physiology and morphology: comparison with intracoronary adenosine. *Circulation.* 1999;100:243–249.
40. Petropoulakis PN, Pavlides GS, Manginas AN, Vassilikos VS, Cokkinos DV. Intracoronary flow velocity measurements in adjacent stenotic and normal coronary arteries during incremental intravenous dobutamine stress and intracoronary adenosine injection. *Catheter Cardiovasc Interv.* 1999;48:1–9.
41. Tadamura E, Iida H, Matsumoto K, et al. Comparison of myocardial blood flow during dobutamine-atropine infusion with that after dipyridamole administration in normal men. *J Am Coll Cardiol.* 2001;37:130–136.
42. Fung AY, Gallagher KP, Buda AJ. The physiologic basis of dobutamine as compared with dipyridamole stress interventions in the assessment of critical coronary stenosis. *Circulation.* 1987;76:943–951.
43. Li D, Dhawale P, Rubin PJ, Haacke EM, Gropler RJ. Myocardial signal response to dipyridamole and dobutamine: demonstration of the BOLD effect using a double-echo gradient-echo sequence. *Magn Reson Med.* 1996;36:16–20.
44. Skopicki HA, Abraham SA, Picard MH, Alpert NM, Fischman AJ, Gewirtz H. Effects of dobutamine at maximally tolerated dose on myocardial blood flow in humans with ischemic heart disease. *Circulation.* 1997;96:3346–3352.
45. Danad I, Uusitalo V, Kero T, et al. Quantitative assessment of myocardial perfusion in the detection of significant coronary artery disease: cutoff values and diagnostic accuracy of quantitative [^{15}O]H_2O PET imaging. *J Am Coll Cardiol.* 2014;64:1464–1475.
46. Farhad H, Dunet V, Bachelard K, Allenbach G, Kaufmann PA, Prior JO. Added prognostic value of myocardial blood flow quantitation in rubidium-82 positron emission tomography imaging. *Eur Heart J Cardiovasc Imaging.* 2013;14:1203–1210.
47. Hajjiri MM, Leavitt MB, Zheng H, Spooner AE, Fischman AJ, Gewirtz H. Comparison of positron emission tomography measurement of adenosine-stimulated absolute myocardial blood flow versus relative myocardial tracer content for physiological assessment of coronary artery stenosis severity and location. *JACC Cardiovasc Imaging.* 2009;2:751–758.
48. Fiechter M, Ghadri JR, Gebhard C, et al. Diagnostic value of ^{13}N-ammonia myocardial perfusion PET: added value of myocardial flow reserve. *J Nucl Med.* 2012;53:1230–1234.
49. Herzog BA, Husmann L, Valenta I, et al. Long-term prognostic value of ^{13}N-ammonia myocardial perfusion positron emission tomography added value of coronary flow reserve. *J Am Coll Cardiol.* 2009;54:150–156.
50. Murthy VL, Naya M, Foster CR, et al. Improved cardiac risk assessment with noninvasive measures of coronary flow reserve. *Circulation.* 2011;124:2215–2224.
51. Parkash R, deKemp RA, Ruddy TD, et al. Potential utility of rubidium 82 PET quantification in patients with 3-vessel coronary artery disease. *J Nucl Cardiol.* 2004;11:440–449.
52. Ziadi MC, Dekemp RA, Williams K, et al. Does quantification of myocardial flow reserve using rubidium-82 positron emission tomography facilitate detection of multivessel coronary artery disease? *J Nucl Cardiol.* 2012;19:670–680.
53. Ziadi MC, Dekemp RA, Williams KA, et al. Impaired myocardial flow reserve on rubidium-82 positron emission tomography imaging predicts adverse outcomes in patients assessed for myocardial ischemia. *J Am Coll Cardiol.* 2011;58:740–748.

54. Murthy VL, Lee BC, Sitek A, et al. Comparison and prognostic validation of multiple methods of quantification of myocardial blood flow with ^{82}Rb PET. *J Nucl Med.* 2014;55:1952–1958.
55. Bhave NM, Freed BH, Yodwut C, et al. Considerations when measuring myocardial perfusion reserve by cardiovascular magnetic resonance using regadenoson. *J Cardiovasc Magn Reson.* 2012;14:89.
56. Gould KL, Pan T, Loghin C, Johnson NP, Guha A, Sdringola S. Frequent diagnostic errors in cardiac PET/CT due to misregistration of CT attenuation and emission PET images: a definitive analysis of causes, consequences, and corrections. *J Nucl Med.* 2007;48:1112–1121.
57. Rajaram M, Tahari AK, Lee AH, et al. Cardiac PET/CT misregistration causes significant changes in estimated myocardial blood flow. *J Nucl Med.* 2013;54: 50–54.
58. Chen GP, Branch KR, Alessio AM, et al. Effect of reconstruction algorithms on myocardial blood flow measurement with ^{13}N-ammonia PET. *J Nucl Med.* 2007;48:1259–1265.
59. Peelukhana SV, Kerr H, Kolli KK, et al. Benefit of cardiac N-13 PET CFR for combined anatomical and functional diagnosis of ischemic coronary artery disease: a pilot study. *Ann Nucl Med.* 2014;28:746–760.
60. Kaufmann PA, Namdar M, Matthew F, et al. Novel Doppler assessment of intracoronary volumetric flow reserve: validation against PET in patients with or without flow-dependent vasodilation. *J Nucl Med.* 2005;46:1272–1277.
61. Merlet P, Mazoyer B, Hittinger L, et al. Assessment of coronary reserve in man: comparison between positron emission tomography with oxygen-15-labeled water and intracoronary Doppler technique. *J Nucl Med.* 1993;34:1899–1904.
62. Miller DD, Donohue TJ, Wolford TL, et al. Assessment of blood flow distal to coronary artery stenoses: correlations between myocardial positron emission tomography and poststenotic intracoronary Doppler flow reserve. *Circulation.* 1996;94:2447–2454.
63. Shelton ME, Senneff MJ, Ludbrook PA, Sobel BE, Bergmann SR. Concordance of nutritive myocardial perfusion reserve and flow velocity reserve in conductance vessels in patients with chest pain with angiographically normal coronary arteries. *J Nucl Med.* 1993;34:717–722.
64. Stewart RE, Miller DD, Bowers TR, et al. PET perfusion and vasodilator function after angioplasty for acute myocardial infarction. *J Nucl Med.* 1997;38: 770–777.
65. Bergmann SR, Herrero P, Markham J, Weinheimer CJ, Walsh MN. Noninvasive quantitation of myocardial blood flow in human subjects with oxygen-15-labeled water and positron emission tomography. *J Am Coll Cardiol.* 1989;14: 639–652.
66. Chareonthaitawee P, Kaufmann PA, Rimoldi O, Camici PG. Heterogeneity of resting and hyperemic myocardial blood flow in healthy humans. *Cardiovasc Res.* 2001;50:151–161.
67. Czernin J, Müller P, Chan S, et al. Influence of age and hemodynamics on myocardial blood flow and flow reserve. *Circulation.* 1993;88:62–69.
68. Prior JO, Schindler TH, Facta AD, et al. Determinants of myocardial blood flow response to cold pressor testing and pharmacologic vasodilation in healthy humans. *Eur J Nucl Med Mol Imaging.* 2007;34:20–27.
69. Quercioli A, Montecucco F, Pataky Z, et al. Improvement in coronary circulatory function in morbidly obese individuals after gastric bypass-induced weight loss: relation to alterations in endocannabinoids and adipocytokines. *Eur Heart J.* 2013;34:2063–2073.
70. Quercioli A, Pataky Z, Vincenti G, et al. Elevated endocannabinoid plasma levels are associated with coronary circulatory dysfunction in obesity. *Eur Heart J.* 2011;32:1369–1378.
71. Tawakol A, Forgione MA, Stuehlinger M, et al. Homocysteine impairs coronary microvascular dilator function in humans. *J Am Coll Cardiol.* 2002;40:1051–1058.
72. Bengel FM. Leaving relativity behind: quantitative clinical perfusion imaging. *J Am Coll Cardiol.* 2011;58:749–751.
73. Sawada S, Muzik O, Beanlands RS, Wolfe E, Hutchins GD, Schwaiger M. Interobserver and interstudy variability of myocardial blood flow and flow-reserve measurements with nitrogen 13 ammonia-labeled positron emission tomography. *J Nucl Cardiol.* 1995;2:413–422.
74. Schindler TH, Schelbert HR, Quercioli A, Dilsizian V. Cardiac PET imaging for the detection and monitoring of coronary artery disease and microvascular health. *JACC Cardiovasc Imaging.* 2010;3:623–640.
75. Tawakol A, Sims K, MacRae C, et al. Myocardial flow regulation in people with mitochondrial myopathy, encephalopathy, lactic acidosis, stroke-like episodes/myoclonic epilepsy and ragged red fibers and other mitochondrial syndromes. *Coron Artery Dis.* 2003;14:197–205.
76. Krivokapich J, Czernin J, Schelbert HR. Dobutamine positron emission tomography: absolute quantitation of rest and dobutamine myocardial blood flow and correlation with cardiac work and percent diameter stenosis in patients with and without coronary artery disease. *J Am Coll Cardiol.* 1996;28:565–572.
77. Krivokapich J, Smith GT, Huang SC, et al. ^{13}N ammonia myocardial imaging at rest and with exercise in normal volunteers: quantification of absolute myocardial perfusion with dynamic positron emission tomography. *Circulation.* 1989; 80:1328–1337.
78. Schindler TH, Nitzsche EU, Olschewski M, et al. PET-measured responses of MBF to cold pressor testing correlate with indices of coronary vasomotion on quantitative coronary angiography. *J Nucl Med.* 2004;45:419–428.
79. Mosher P, Ross J, McFate PA, Shaw RF. Control of coronary blood flow by an autoregulatory mechanism. *Circ Res.* 1964;14:250–259.
80. Schindler TH, Zhang X, Vincenti G, et al. Diagnostic value of PET-measured heterogeneity in myocardial blood flows during cold pressor testing for the identification of coronary vasomotor dysfunction. *J Nucl Cardiol.* 2007;14:688–697.
81. Uren NG, Camici PG, Melin JA, et al. Effect of aging on myocardial perfusion reserve. *J Nucl Med.* 1995;36:2032–2036.
82. Duvernoy CS, Rattenhuber J, Seifert-Klauss V, Bengel F, Meyer C, Schwaiger M. Myocardial blood flow and flow reserve in response to short-term cyclical hormone replacement therapy in postmenopausal women. *J Gend Specif Med.* 2001;4:21–27, 47.
83. Duvernoy CS, Meyer C, Seifert-Klauss V, et al. Gender differences in myocardial blood flow dynamics: lipid profile and hemodynamic effects. *J Am Coll Cardiol.* 1999;33:463–470.
84. Motivala AA, Rose PA, Kim HM, et al. Cardiovascular risk, obesity, and myocardial blood flow in postmenopausal women. *J Nucl Cardiol.* 2008;15:510–517.
85. Uren NG, Melin JA, De Bruyne B, Wijns W, Baudhuin T, Camici PG. Relation between myocardial blood flow and the severity of coronary-artery stenosis. *N Engl J Med.* 1994;330:1782–1788.
86. Beanlands RSB, Muzik O, Melon P, et al. Noninvasive quantification of regional myocardial flow reserve in patients with coronary atherosclerosis using nitrogen-13 ammonia positron emission tomography: determination of extent of altered vascular reactivity. *J Am Coll Cardiol.* 1995;26:1465–1475.
87. Di Carli M, Czernin J, Hoh CK, et al. Relation among stenosis severity, myocardial blood flow, and flow reserve in patients with coronary artery disease. *Circulation.* 1995;91:1944–1951.
88. Muzik O, Duvernoy C, Beanlands RSB, et al. Assessment of diagnostic performance of quantitative flow measurements in normal subjects and patients with angiographically documented coronary artery disease by means of nitrogen-13 ammonia and positron emission tomography. *J Am Coll Cardiol.* 1998;31:534–540.
89. Anagnostopoulos C, Almonacid A, Fakhri G, et al. Quantitative relationship between coronary vasodilator reserve assessed by ^{82}Rb PET imaging and coronary artery stenosis severity. *Eur J Nucl Med Mol Imaging.* 2008;35:1593–1601.
90. Yoshinaga K, Katoh C, Manabe O, et al. Incremental diagnostic value of regional myocardial blood flow quantification over relative perfusion imaging with generator-produced rubidium-82 PET. *Circ J.* 2011;75:2628–2634.
91. Naya M, Murthy VL, Taqueti VR, et al. Preserved coronary flow reserve effectively excludes high-risk coronary artery disease on angiography. *J Nucl Med.* 2014;55:248–255.
92. Fukushima K, Javadi MS, Higuchi T, et al. Prediction of short-term cardiovascular events using quantification of global myocardial flow reserve in patients referred for clinical ^{82}Rb PET perfusion imaging. *J Nucl Med.* 2011;52:726–732.
93. Slart RHJA, Zeebregts CJ, Hillege HL, et al. Myocardial perfusion reserve after a PET-driven revascularization procedure: a strong prognostic factor. *J Nucl Med.* 2011;52:873–879.
94. Tio RA, Dabeshlim A, Siebelink H-MJ, et al. Comparison between the prognostic value of left ventricular function and myocardial perfusion reserve in patients with ischemic heart disease. *J Nucl Med.* 2009;50:214–219.
95. Di Carli MF, Murthy VL. Cardiac PET/CT for the evaluation of known or suspected coronary artery disease. *Radiographics.* 2011;31:1239–1254.
96. Hachamovitch R, Rozanski A, Shaw LJ, et al. Impact of ischaemia and scar on the therapeutic benefit derived from myocardial revascularization vs. medical therapy among patients undergoing stress-rest myocardial perfusion scintigraphy. *Eur Heart J.* 2011;32:1012–1024.
97. Gould KL, Johnson NP, Kaul S, et al. Patient selection for elective revascularization to reduce myocardial infarction and mortality: new lessons from randomized trials, coronary physiology, and statistics. *Circ Cardiovasc Imaging.* 2015;8:e003099.
98. Taqueti VR, Hachamovitch R, Murthy VL, et al. Global coronary flow reserve is associated with adverse cardiovascular events independently of luminal angiographic severity and modifies the effect of early revascularization. *Circulation.* 2015;131:19–27.

99. Grundy SM, Benjamin IJ, Burke GL, et al. Diabetes and cardiovascular disease: a statement for healthcare professionals from the American Heart Association. *Circulation.* 1999;100:1134–1146.
100. Rajagopalan N, Miller TD, Hodge DO, Frye RL, Gibbons RJ. Identifying high-risk asymptomatic diabetic patients who are candidates for screening stress single-photon emission computed tomography imaging. *J Am Coll Cardiol.* 2005;45:43–49.
101. Shaw LJ, Iskandrian A. Prognostic value of gated myocardial perfusion SPECT. *J Nucl Cardiol.* 2004;11:171–185.
102. Murthy VL, Naya M, Foster CR, et al. Association between coronary vascular dysfunction and cardiac mortality in patients with and without diabetes mellitus. *Circulation.* 2012;126:1858–1868.
103. U.S. Renal Data System. *USRDS 2010 Annual Data Report: Atlas of Chronic Kidney Disease and End-Stage Renal Disease in the United States*. Bethesda, MD: National Institutes of Health, National Institute of Diabetes and Digestive and Kidney Diseases; 2010.
104. Charytan DM, Wallentin L, Lagerqvist B, et al. Early angiography in patients with chronic kidney disease: a collaborative systematic review. *Clin J Am Soc Nephrol.* 2009;4:1032–1043.
105. Gruberg L, Mintz GS, Mehran R, et al. The prognostic implications of further renal function deterioration within 48 h of interventional coronary procedures in patients with pre-existent chronic renal insufficiency. *J Am Coll Cardiol.* 2000;36:1542–1548.
106. Cooper WA, O'Brien SM, Thourani VH, et al. Impact of renal dysfunction on outcomes of coronary artery bypass surgery. *Circulation.* 2006;113:1063–1070.
107. Shin D-H, Choi D-J, Youn T-J, et al. Comparison of contrast-induced nephrotoxicity of iodixanol and iopromide in patients with renal insufficiency undergoing coronary angiography. *Am J Cardiol.* 2011;108:189–194.
108. Al-Mallah MH, Hachamovitch R, Dorbala S, Di Carli MF. Incremental prognostic value of myocardial perfusion imaging in patients referred to stress single-photon emission computed tomography with renal dysfunction. *Circ Cardiovasc Imaging.* 2009;2:429–436.
109. Murthy VL, Naya M, Foster CR, et al. Coronary vascular dysfunction and prognosis in patients with chronic kidney disease. *JACC Cardiovasc Imaging.* 2012;5:1025–1034.
110. Shah NR, Charytan DM, Murthy VL, et al. Prognostic value of coronary flow reserve in patients with dialysis-dependent ESRD. *J Am Soc Nephrol.* 2016;27:1823–1829.
111. Majmudar MD, Murthy VL, Shah RV, et al. Quantification of coronary flow reserve in patients with ischaemic and non-ischaemic cardiomyopathy and its association with clinical outcomes. *Eur Heart J Cardiovasc Imaging.* 2015;16:900–909.
112. Bratis K, Child N, Terrovitis J, et al. Coronary microvascular dysfunction in overt diabetic cardiomyopathy. *IJC Metab Endocr.* 2014;5:19–23.
113. Cecchi F, Olivotto I, Gistri R, Lorenzoni R, Chiriatti G, Camici PG. Coronary microvascular dysfunction and prognosis in hypertrophic cardiomyopathy. *N Engl J Med.* 2003;349:1027–1035.
114. Dorbala S, Vangala D, Bruyere J, et al. Coronary microvascular dysfunction is related to abnormalities in myocardial structure and function in cardiac amyloidosis. *JACC Heart Fail.* 2014;2:358–367.
115. Kalliokoski RJ, Kalliokoski KK, Sundell J, et al. Impaired myocardial perfusion reserve but preserved peripheral endothelial function in patients with Fabry disease. *J Inherit Metab Dis.* 2005;28:563–573.
116. Neglia D, Michelassi C, Trivieri MG, et al. Prognostic role of myocardial blood flow impairment in idiopathic left ventricular dysfunction. *Circulation.* 2002; 105:186–193.
117. Kofoed KF, Czernin J, Johnson J, et al. Effects of cardiac allograft vasculopathy on myocardial blood flow, vasodilatory capacity, and coronary vasomotion. *Circulation.* 1997;95:600–606.
118. Treasure CB, Vita J, Ganz P, et al. Loss of the coronary microvascular response to acetylcholine in cardiac transplant patients. *Circulation.* 1992;86:1156–1164.
119. Spes CH, Klauss V, Mudra H, et al. Diagnostic and prognostic value of serial dobutamine stress echocardiography for noninvasive assessment of cardiac allograft vasculopathy: a comparison with coronary angiography and intravascular ultrasound. *Circulation.* 1999;100:509–515.
120. Spes CH, Mudra H, Schnaack SD, et al. Dobutamine stress echocardiography for noninvasive diagnosis of cardiac allograft vasculopathy: a comparison with angiography and intravascular ultrasound. *Am J Cardiol.* 1996;78:168–174.
121. Thompson D, Koster MJ, Wagner RH, Heroux A, Barron JT. Single photon emission computed tomography myocardial perfusion imaging to detect cardiac allograft vasculopathy. *Eur Heart J Cardiovasc Imaging.* 2012;13:271–275.
122. Manrique A, Bernard M, Hitzel A, et al. Diagnostic and prognostic value of myocardial perfusion gated SPECT in orthotopic heart transplant recipients. *J Nucl Cardiol.* 2010;17:197–206.
123. Hacker M, Hoyer HX, Uebleis C, et al. Quantitative assessment of cardiac allograft vasculopathy by real-time myocardial contrast echocardiography: a comparison with conventional echocardiographic analyses and [Tc99m]-sestamibi SPECT. *Eur J Echocardiogr.* 2008;9:494–500.
124. Kübrich M, Petrakopoulou P, Kofler S, et al. Impact of coronary endothelial dysfunction on adverse long-term outcome after heart transplantation. *Transplantation.* 2008;85:1580–1587.
125. Wu Y-W, Chen Y-H, Wang S-S, et al. PET assessment of myocardial perfusion reserve inversely correlates with intravascular ultrasound findings in angiographically normal cardiac transplant recipients. *J Nucl Med.* 2010;51:906–912.
126. Allen-Auerbach M, Schöder H, Johnson J, et al. Relationship between coronary function by positron emission tomography and temporal changes in morphology by intravascular ultrasound (IVUS) in transplant recipients. *J Heart Lung Transplant.* 1999;18:211–219.
127. Mc Ardle BA, Davies RA, Chen L, et al. Prognostic value of rubidium-82 positron emission tomography in patients after heart transplant. *Circ Cardiovasc Imaging.* 2014;7:930–937.
128. Jaeger BR, Bengel FM, Odaka K, et al. Changes in myocardial vasoreactivity after drastic reduction of plasma fibrinogen and cholesterol: a clinical study in long-term heart transplant survivors using positron emission tomography. *J Heart Lung Transplant.* 2005;24:2022–2030.
129. Kushwaha SS, Narula J, Narula N, et al. Pattern of changes over time in myocardial blood flow and microvascular dilator capacity in patients with normally functioning cardiac allografts. *Am J Cardiol.* 1998;82:1377–1381.
130. Preumont N, Berkenboom G, Vachiery J, et al. Early alterations of myocardial blood flow reserve in heart transplant recipients with angiographically normal coronary arteries. *J Heart Lung Transplant.* 2000;19:538–545.
131. Murthy V, Naya M, Hachamovitch R, et al. Coronary vascular dysfunction and prognosis in patients age 75 and older [abstract]. *J Nucl Med.* 2012;53(suppl 1):22.
132. Mieres JH, Shaw LJ, Hendel RC, et al. American Society of Nuclear Cardiology consensus statement: Task Force on Women and Coronary Artery Disease—the role of myocardial perfusion imaging in the clinical evaluation of coronary artery disease in women [correction]. *J Nucl Cardiol.* 2003; 10:95–101.
133. Taqueti VR, Dorbala S, Wolinsky D, et al. Myocardial perfusion imaging in women for the evaluation of stable ischemic heart disease: state-of-the-evidence and clinical recommendations. *J Nucl Cardiol.* June 5, 2017 [Epub ahead of print].
134. Johnson BD, Shaw LJ, Buchthal SD, et al. Prognosis in women with myocardial ischemia in the absence of obstructive coronary disease: results from the National Institutes of Health–National Heart, Lung, and Blood Institute–Sponsored Women's Ischemia Syndrome Evaluation (WISE). *Circulation.* 2004;109:2993–2999.
135. Pepine CJ, Anderson RD, Sharaf BL, et al. Coronary microvascular reactivity to adenosine predicts adverse outcome in women evaluated for suspected ischemia: results from the National Heart, Lung and Blood Institute WISE (Women's Ischemia Syndrome Evaluation) study. *J Am Coll Cardiol.* 2010;55:2825–2832.
136. Taqueti VR, Shaw LJ, Cook NR, et al. Excess cardiovascular risk in women relative to men referred for coronary angiography is associated with severely impaired coronary flow reserve, not obstructive disease. *Circulation.* 2017;135: 566–577.
137. Murthy VL, Naya M, Taqueti VR, et al. Effects of sex on coronary microvascular dysfunction and cardiac outcomes. *Circulation.* 2014;129:2518–2527.
138. Naya M, Murthy VL, Foster CR, et al. Prognostic interplay of coronary artery calcification and underlying vascular dysfunction in patients with suspected coronary artery disease. *J Am Coll Cardiol.* 2013;61:2098–2106.
139. Gould KL, Lipscomb K, Hamilton GW. Physiologic basis for assessing critical coronary stenosis: instantaneous flow response and regional distribution during coronary hyperemia as measures of coronary flow reserve. *Am J Cardiol.* 1974;33:87–94.
140. Gould KL, Lipscomb K. Effects of coronary stenoses on coronary flow reserve and resistance. *Am J Cardiol.* 1974;34:48–55.
141. Fiechter M, Gebhard C, Ghadri JR, et al. Myocardial perfusion imaging with ^{13}N-ammonia PET is a strong predictor for outcome. *Int J Cardiol.* 2013;167: 1023–1026.
142. Morton G, Chiribiri A, Ishida M, et al. Quantification of absolute myocardial perfusion in patients with coronary artery disease: comparison between cardiovascular magnetic resonance and positron emission tomography. *J Am Coll Cardiol.* 2012;60:1546–1555.
143. Di Carli MF, Charytan D, McMahon GT, Ganz P, Dorbala S, Schelbert HR. Coronary circulatory function in patients with the metabolic syndrome. *J Nucl Med.* 2011;52:1369–1377.
144. Di Carli MF, Janisse J, Ager J, Grunberger G. Role of chronic hyperglycemia in the pathogenesis of coronary microvascular dysfunction in diabetes. *J Am Coll Cardiol.* 2003;41:1387–1393.

145. Di Carli MF, Bianco-Batlles D, Landa ME, et al. Effects of autonomic neuropathy on coronary blood flow in patients with diabetes mellitus. *Circulation.* 1999;100:813–819.
146. Kaufmann PA, Gnecchi-Ruscone T, Schäfers KP, Lüscher TF, Camici PG. Low density lipoprotein cholesterol and coronary microvascular dysfunction in hypercholesterolemia. *J Am Coll Cardiol.* 2000;36:103–109.
147. Pitkänen O-P, Nuutila P, Raitakari OT, et al. Coronary flow reserve is reduced in young men with IDDM. *Diabetes.* 1998;47:248–254.
148. Prior JO, Quiñones MJ, Hernandez-Pampaloni M, et al. Coronary circulatory dysfunction in insulin resistance, impaired glucose tolerance, and type 2 diabetes mellitus. *Circulation.* 2005;111:2291–2298.
149. Quiñones MJ, Hernandez-Pampaloni M, Schelbert H, et al. Coronary vasomotor abnormalities in insulin-resistant individuals. *Ann Intern Med.* 2004;140:700–708.
150. Rana O, Byrne CD, Kerr D, et al. Acute hypoglycemia decreases myocardial blood flow reserve in patients with type 1 diabetes mellitus and in healthy humans. *Circulation.* 2011;124:1548–1556.
151. von Scholten BJ, Hasbak P, Christensen TE, et al. Cardiac ^{82}Rb PET/CT for fast and non-invasive assessment of microvascular function and structure in asymptomatic patients with type 2 diabetes. *Diabetologia.* 2016;59:371–8.
152. Valenta I, Dilsizian V, Quercioli A, Schelbert H, Schindler T. The influence of insulin resistance, obesity, and diabetes mellitus on vascular tone and myocardial blood flow. *Curr Cardiol Rep.* 2012;14:217–225.
153. Yokoyama I, Ohtake T, Momomura S, et al. Hyperglycemia rather than insulin resistance is related to reduced coronary flow reserve in NIDDM. *Diabetes.* 1998;47:119–124.
154. Yokoyama I, Momomura S, Ohtake T, et al. Reduced myocardial flow reserve in non-insulin-dependent diabetes mellitus. *J Am Coll Cardiol.* 1997;30:1472–1477.
155. Alexánderson E, Jácome R, Jiménez-Santos M, et al. Evaluation of the endothelial function in hypertensive patients with ^{13}N-ammonia PET. *J Nucl Cardiol.* 2012;19:979–986.
156. Hamasaki S, Al Suwaidi J, Higano ST, Miyauchi K, Holmes DR Jr, Lerman A. Attenuated coronary flow reserve and vascular remodeling in patients with hypertension and left ventricular hypertrophy. *J Am Coll Cardiol.* 2000;35:1654–1660.
157. Houghton JL, Frank MJ, Carr AA, von Dohlen TW, Prisant LM. Relations among impaired coronary flow reserve, left ventricular hypertrophy and thallium perfusion defects in hypertensive patients without obstructive coronary artery disease. *J Am Coll Cardiol.* 1990;15:43–51.
158. Laine H, Raitakari OT, Niinikoski H, et al. Early impairment of coronary flow reserve in young men with borderline hypertension. *J Am Coll Cardiol.* 1998;32:147–153.
159. Dayanikli F, Grambow D, Muzik O, Mosca L, Rubenfire M, Schwaiger M. Early detection of abnormal coronary flow reserve in asymptomatic men at high risk for coronary artery disease using positron emission tomography. *Circulation.* 1994;90:808–817.
160. Yokoyama I, Ohtake T, Momomura S, et al. Impaired myocardial vasodilation during hyperemic stress with dipyridamole in hypertriglyceridemia. *J Am Coll Cardiol.* 1998;31:1568–1574.
161. Yokoyama I, Ohtake T, Momomura S, et al. Altered myocardial vasodilatation in patients with hypertriglyceridemia in anatomically normal coronary arteries. *Arterioscler Thromb Vasc Biol.* 1998;18:294–299.
162. Yokoyama I, Ohtake T, Momomura S, Nishikawa J, Sasaki Y, Omata M. Reduced coronary flow reserve in hypercholesterolemic patients without overt coronary stenosis. *Circulation.* 1996;94:3232–3238.
163. Yokoyama I, Murakami T, Ohtake T, et al. Reduced coronary flow reserve in familial hypercholesterolemia. *J Nucl Med.* 1996;37:1937–1942.
164. Bozbas H, Pirat B, Demirtas S, et al. Evaluation of coronary microvascular function in patients with end-stage renal disease, and renal allograft recipients. *Atherosclerosis.* 2009;202:498–504.
165. Charytan DM, Shelbert HR, Di Carli MF. Coronary microvascular function in early chronic kidney disease. *Circ Cardiovasc Imaging.* 2010;3:663–671.
166. Goldstein RA, Kirkeeide RL, Demer LL, et al. Relation between geometric dimensions of coronary artery stenoses and myocardial perfusion reserve in man. *J Clin Invest.* 1987;79:1473–1478.
167. Kirkeeide RL, Gould KL, Parsel L. Assessment of coronary stenoses by myocardial perfusion imaging during pharmacologic coronary vasodilation. VII. Validation of coronary flow reserve as a single integrated functional measure of stenosis severity reflecting all its geometric dimensions. *J Am Coll Cardiol.* 1986;7:103–113.
168. Gould KL, Nakagawa Y, Nakagawa K, et al. Frequency and clinical implications of fluid dynamically significant diffuse coronary artery disease manifest as graded, longitudinal, base-to-apex myocardial perfusion abnormalities by noninvasive positron emission tomography. *Circulation.* 2000;101:1931–1939.
169. Arnett EN, Isner JM, Redwood DR, et al. Coronary artery narrowing in coronary heart disease: comparison of cineangiographic and necropsy findings. *Ann Intern Med.* 1979;91:350–356.
170. Nicholls SJ, Tuzcu EM, Crowe T, et al. Relationship between cardiovascular risk factors and atherosclerotic disease burden measured by intravascular ultrasound. *J Am Coll Cardiol.* 2006;47:1967–1975.
171. Johnson NP, Gould KL. Integrating noninvasive absolute flow, coronary flow reserve, and ischemic thresholds into a comprehensive map of physiological severity. *JACC Cardiovasc Imaging.* 2012;5:430–440.
172. Naya M, Murthy VL, Blankstein R, et al. Quantitative relationship between the extent and morphology of coronary atherosclerotic plaque and downstream myocardial perfusion. *J Am Coll Cardiol.* 2011;58:1807–1816.
173. Dey D, Diaz Zamudio M, Schuhbaeck A, et al. Relationship between quantitative adverse plaque features from coronary computed tomography angiography and downstream impaired myocardial flow reserve by ^{13}N-ammonia positron emission tomography: a pilot study. *Circ Cardiovasc Imaging.* 2015;8:e003255.
174. Danad I, Raijmakers PG, Appelman YE, et al. Hybrid imaging using quantitative $H_2{}^{15}O$ PET and CT-based coronary angiography for the detection of coronary artery disease. *J Nucl Med.* 2013;54:55–63.
175. Liga R, Marini C, Coceani M, et al. Structural abnormalities of the coronary arterial wall—in addition to luminal narrowing—affect myocardial blood flow reserve. *J Nucl Med.* 2011;52:1704–1712.
176. Kim H-S, Cho S-G, Kim JH, Bom H-S. Indirect radionuclide coronary angiography to evaluate gradients of myocardial blood flow and flow reserve through coronary stenosis using N-13 ammonia PET/CT. *Chonnam Med J.* 2013;49:69–74.
177. Bateman TM, Gould KL, Carli MFD. Proceedings of the Cardiac PET Summit, 12 May 2014, Baltimore, MD: 3: Quantification of myocardial blood flow. *J Nucl Cardiol.* 2015;22:571–578.
178. Juneau D, Erthal F, Ohira H, et al. Clinical PET myocardial perfusion imaging and flow quantification. *Cardiol Clin.* 2016;34:69–85.
179. Topol EJ, Nissen SE. Our preoccupation with coronary luminology: the dissociation between clinical and angiographic findings in ischemic heart disease. *Circulation.* 1995;92:2333–2342.
180. Meijboom WB, Van Mieghem CAG, van Pelt N, et al. Comprehensive assessment of coronary artery stenoses: computed tomography coronary angiography versus conventional coronary angiography and correlation with fractional flow reserve in patients with stable angina. *J Am Coll Cardiol.* 2008;52:636–643.
181. Toth G, Hamilos M, Pyxaras S, et al. Evolving concepts of angiogram: fractional flow reserve discordances in 4000 coronary stenoses. *Eur Heart J.* 2014;35:2831–2838.
182. Min JK, Taylor CA, Achenbach S, et al. Noninvasive fractional flow reserve derived from coronary CT angiography: clinical data and scientific principles. *JACC Cardiovasc Imaging.* 2015;8:1209–1222.
183. Pijls NH, Van Son JA, Kirkeeide RL, De Bruyne B, Gould KL. Experimental basis of determining maximum coronary, myocardial, and collateral blood flow by pressure measurements for assessing functional stenosis severity before and after percutaneous transluminal coronary angioplasty. *Circulation.* 1993;87:1354–1367.
184. Pijls NHJ, de Bruyne B, Peels K, et al. Measurement of fractional flow reserve to assess the functional severity of coronary-artery stenoses. *N Engl J Med.* 1996;334:1703–1708.
185. De Bruyne B, Paulus WJ, Vantrimpont PJ, Sys SU, Heyndrickx GR, Pijls NHJ. Transstenotic coronary pressure gradient measurement in humans: in vitro and in vivo evaluation of a new pressure monitoring angioplasty guide wire. *J Am Coll Cardiol.* 1993;22:119–126.
186. De Bruyne B, Baudhuin T, Melin JA, et al. Coronary flow reserve calculated from pressure measurements in humans: validation with positron emission tomography. *Circulation.* 1994;89:1013–1022.
187. Tonino PA, De Bruyne B, Pijls N. Fractional flow reserve versus angiography for guiding percutaneous coronary intervention. *N Engl J Med.* 2009;360:213–224.
188. De Bruyne B, Pijls NHJ, Kalesan B, et al. Fractional flow reserve–guided PCI versus medical therapy in stable coronary disease. *N Engl J Med.* 2012;367:991–1001.
189. Pijls NHJ, van Schaardenburgh P, Manoharan G, et al. Percutaneous coronary intervention of functionally nonsignificant stenosis: 5-year follow-up of the DEFER study. *J Am Coll Cardiol.* 2007;49:2105–2111.
190. van de Hoef TP, Siebes M. Spaan JA, Piek JJ. Fundamentals in clinical coronary physiology: why coronary flow is more important than coronary pressure. *Eur Heart J.* 2015;36:3312–3319.
191. Blows LJ, Redwood SR. The pressure wire in practice. *Heart.* 2007;93:419–422.
192. Plein S, Motwani M. Fractional flow reserve as the reference standard for myocardial perfusion studies: fool's gold? *Eur Heart J Cardiovasc Imaging.* 2013;14:1211–1213.

193. van de Hoef TP, Bax M, Damman P, et al. Impaired coronary autoregulation is associated with long-term fatal events in patients with stable coronary artery disease. *Circ Cardiovasc Interv.* 2013;6:329–335.
194. van de Hoef TP, van Lavieren MA, Damman P, et al. Physiological basis and long-term clinical outcome of discordance between fractional flow reserve and coronary flow velocity reserve in coronary stenoses of intermediate severity. *Circ Cardiovasc Interv.* 2014;7:301–311.
195. De Bruyne B, Hersbach F, Pijls NHJ, et al. Abnormal epicardial coronary resistance in patients with diffuse atherosclerosis but "normal" coronary angiography. *Circulation.* 2001;104:2401–2406.
196. Hwang D, Jeon K-H, Lee JM, et al. Diagnostic performance of resting and hyperemic invasive physiological indices to define myocardial ischemia: validation with ^{13}N-ammonia positron emission tomography. *JACC Cardiovasc Interv.* 2017;10:751–760.
197. Hennigan B, Oldroyd KG, Berry C, et al. Discordance between resting and hyperemic indices of coronary stenosis severity: the VERIFY 2 study (a comparative study of resting coronary pressure gradient, instantaneous wave-free ratio and fractional flow reserve in an unselected population referred for invasive angiography). *Circ Cardiovasc Interv.* 2016;9:e004016.
198. Johnson NP, Kirkeeide RL, Asrress KN, et al. Does the instantaneous wave-free ratio approximate the fractional flow reserve? *J Am Coll Cardiol.* 2013;61:1428–1435.
199. Jeremias A, Maehara A, Généreux P, et al. Multicenter core laboratory comparison of the instantaneous wave-free ratio and resting Pd/Pa with fractional flow reserve: the RESOLVE study. *J Am Coll Cardiol.* 2014;63:1253–1261.
200. Götberg M, Christiansen EH, Gudmundsdottir IJ, et al. Instantaneous wave-free ratio versus fractional flow reserve to guide PCI. *N Engl J Med.* 2017;376:1813–1823.
201. Davies JE, Sen S, Dehbi H-M, et al. Use of the instantaneous wave-free ratio or fractional flow reserve in PCI. *N Engl J Med.* 2017;376:1824–1834.
202. Dilsizian V, Bacharach SL, Beanlands RS, et al. ASNC imaging guidelines/SNMMI procedure standard for positron emission tomography (PET) nuclear cardiology procedures. *J Nucl Cardiol.* 2016;23:1187–1226.
203. Barbato E, Aarnoudse W, Aengevaeren WR, et al. Validation of coronary flow reserve measurements by thermodilution in clinical practice. *Eur Heart J.* 2004;25:219–223.
204. Escaned J, Echavarría-Pinto M. Moving beyond coronary stenosis: has the time arrived to address important physiological questions not answered by fractional flow reserve alone? *Circ Cardiovasc Interv.* 2014;7:282–284.
205. Wada T, Hirata K, Shiono Y, et al. Coronary flow velocity reserve in three major coronary arteries by transthoracic echocardiography for the functional assessment of coronary artery disease: a comparison with fractional flow reserve. *Eur Heart J Cardiovasc Imaging.* 2014;15:399–408.
206. Gaibazzi N, Rigo F, Lorenzoni V, et al. Comparative prediction of cardiac events by wall motion, wall motion plus coronary flow reserve, or myocardial perfusion analysis: a multicenter study of contrast stress echocardiography. *JACC Cardiovasc Imaging.* 2013;6:1–12.
207. Wu J, Barton D, Xie F, et al. Comparison of fractional flow reserve assessment with demand stress myocardial contrast echocardiography in angiographically intermediate coronary stenoses. *Circ Cardiovasc Imaging.* 2016;9:e004129.
208. Leung DY, Leung M. Non-invasive/invasive imaging: significance and assessment of coronary microvascular dysfunction. *Heart.* 2011;97:587–595.
209. Combined Pressure and Flow Measurements to Guide Treatment of Coronary Stenoses (DEFINE-FLOW). ClinicalTrials.gov website. https://clinicaltrials.gov/ct2/show/NCT02328820. Published December 18, 2014. Updated May 12, 2016. Accessed September 14, 2017.
210. Johnson NP, Kirkeeide RL, Gould KL. Is discordance of coronary flow reserve and fractional flow reserve due to methodology or clinically relevant coronary pathophysiology? *JACC Cardiovasc Imaging.* 2012;5:193–202.
211. Johnson NP, Gould KL. Regadenoson versus dipyridamole hyperemia for cardiac PET imaging. *JACC Cardiovasc Imaging.* 2015;8:438–447.
212. Hutchins GD, Schwaiger M, Rosenspire KC, Krivokapich J, Schelbert H, Kuhl DE. Noninvasive quantification of regional blood flow in the human heart using N-13 ammonia and dynamic positron emission tomographic imaging. *J Am Coll Cardiol.* 1990;15:1032–1042.
213. Chan SY, Brunken RC, Czernin J, et al. Comparison of maximal myocardial blood flow during adenosine infusion with that of intravenous dipyridamole in normal men. *J Am Coll Cardiol.* 1992;20:979–985.
214. Böttcher M, Czernin J, Sun K, Phelps ME, Schelbert HR. Effect of β1 adrenergic receptor blockade on myocardial blood flow and vasodilatory capacity. *J Nucl Med.* 1997;38:442–446.
215. Campisi R, Czernin J, Karpman HL, Schelbert HR. Coronary vasodilatory capacity and flow reserve in normal myocardium supplied by bypass grafts late after surgery. *Am J Cardiol.* 1997;80:27–31.
216. Nitzsche EU, Choi Y, Czernin J, Hoh CK, Huang S-C, Schelbert HR. Noninvasive quantification of myocardial blood flow in humans: a direct comparison of the [^{13}N]ammonia and the [^{15}O]water techniques. *Circulation.* 1996;93:2000–2006.
217. Muzik O, Paridon SM, Singh TP, Morrow WR, Dayanikli F, Di Carli MF. Quantification of myocardial blood flow and flow reserve in children with a history of Kawasaki disease and normal coronary arteries using positron emission tomography. *J Am Coll Cardiol.* 1996;28:757–762.
218. DeGrado TR, Hanson MW, Turkington TG, et al. Estimation of myocardial blood flow for longitudinal studies with ^{13}N-labeled ammonia and positron emission tomography. *J Nucl Cardiol.* 1996;3:494–507.
219. Schindler TH, Cardenas J, Prior JO, et al. Relationship between increasing body weight, insulin resistance, inflammation, adipocytokine leptin, and coronary circulatory function. *J Am Coll Cardiol.* 2006;47:1188–1195.
220. Valenta I, Quercioli A, Vincenti G, et al. Structural epicardial disease and microvascular function are determinants of an abnormal longitudinal myocardial blood flow difference in cardiovascular risk individuals as determined with PET/CT. *J Nucl Cardiol.* 2010;17:1023–1033.
221. Renaud JM, Dasilva JN, Beanlands RSB, Dekemp RA. Characterizing the normal range of myocardial blood flow with ^{82}rubidium and ^{13}N-ammonia PET imaging. *J Nucl Cardiol.* 2013;20:578–591.
222. Lin JW, Sciacca RR, Chou RL, Laine AF, Bergmann SR. Quantification of myocardial perfusion in human subjects using ^{82}Rb and wavelet-based noise reduction. *J Nucl Med.* 2001;42:201–208.
223. Manabe O, Yoshinaga K, Katoh C, Naya M, deKemp RA, Tamaki N. Repeatability of rest and hyperemic myocardial blood flow measurements with ^{82}Rb dynamic PET. *J Nucl Med.* 2009;50:68–71.
224. Prior JO, Allenbach G, Valenta I, et al. Quantification of myocardial blood flow with ^{82}Rb positron emission tomography: clinical validation with ^{15}O-water. *Eur J Nucl Med Mol Imaging.* 2012;39:1037–1047.
225. Sdringola S, Johnson NP, Kirkeeide RL, Cid E, Gould KL. Impact of unexpected factors on quantitative myocardial perfusion and coronary flow reserve in young, asymptomatic volunteers. *JACC Cardiovasc Imaging.* 2011;4:402–412.
226. Germino M, Ropchan J, Mulnix T, et al. Quantification of myocardial blood flow with ^{82}Rb: validation with ^{15}O-water using time-of-flight and point-spread-function modeling. *EJNMMI Res.* 2016;6:68.
227. Farhad H, Murthy VL. Pharmacologic manipulation of coronary vascular physiology for the evaluation of coronary artery disease. *Pharmacol Ther.* 2013;149:121–132.
228. Nienaber CA, Ratib O, Gambhir SS, et al. A quantitative index of regional blood flow in canine myocardium derived noninvasively with N-13 ammonia and dynamic positron emission tomography. *J Am Coll Cardiol.* 1991;17:260–269.
229. Schelbert HR, Phelps ME, Hoffman E, Huang S-C, Kuhl DE. Regional myocardial blood flow, metabolism and function assessed noninvasively with positron emission tomography. *Am J Cardiol.* 1980;46:1269–1277.
230. De Bruyne B, Oldroyd KG, Pijls NHJ. Microvascular (dys)function and clinical outcome in stable coronary disease. *J Am Coll Cardiol.* 2016;67:1170–1172.

JNM The Journal of NUCLEAR MEDICINE

Clinical Quantification of Myocardial Blood Flow Using PET: Joint Position Paper of the SNMMI Cardiovascular Council and the ASNC

Venkatesh L. Murthy, Timothy M. Bateman, Rob S. Beanlands, Daniel S. Berman, Salvador Borges-Neto, Panithaya Chareonthaitawee, Manuel D. Cerqueira, Robert A. deKemp, E. Gordon DePuey, Vasken Dilsizian, Sharmila Dorbala, Edward P. Ficaro, Ernest V. Garcia, Henry Gewirtz, Gary V. Heller, Howard C. Lewin, Saurabh Malhotra, April Mann, Terrence D. Ruddy, Thomas H. Schindler, Ronald G. Schwartz, Piotr J. Slomka, Prem Soman and Marcelo F. Di Carli

J Nucl Med. 2018;59:273-293.
Published online: December 14, 2017.
Doi: 10.2967/jnumed.117.201368

The Journal of Nuclear Medicine is published monthly.
SNMMI | Society of Nuclear Medicine and Molecular Imaging
1850 Samuel Morse Drive, Reston, VA 20190.
(Print ISSN: 0161-5505, Online ISSN: 2159-662X)

SNMMI SOCIETY OF NUCLEAR MEDICINE AND MOLECULAR IMAGING